J. Indian Inst. Sci.
A Multidisciplinary Reviews Journal
ISSN: 0970-4140 Coden-JIISAD

REVIEW ARTICLE

Small-Scale Flow with Deformable Boundaries

Pratyaksh Karan, Jeevanjyoti Chakraborty and Suman Chakraborty*

Abstract | In this article, we present an overview of research on flow in microconfinements with deformable boundaries. The time frame of focus is the last decade (2007–2017). The article is arranged into sections based on the geometry of the problem studied, which fall under five major categories—microchannels, tubes, squeeze flow, cylinder near wall and thin structures (membranes, sheets, etc.). The modelling of various coupled phenomena such as electrokinetics, diffusion and porous flow is discussed, maintaining the study of deformable boundaries as a common underlying theme. The article concludes with a brief discussion about the cross-correlation between the works presented based on the phenomena studied, constitutive models considered and methodologies employed.

Keywords: *Micro-confinement, Fluid–structure interactions, Microfluidics, Deformation, Deflection, Elasticity*

1 Introduction

Study of flows at small scales has been one of the major aspects of fluid mechanics research since its advent, and it has received an impetus in the last two decades because of improved experimental technologies, better understanding of the fundamentals and increasing requirements from industry and society. Furthermore, at the small length scales (10 nm–0.1 mm), other physical effects have significant contributions to the system being probed, examples being electrokinetics, species diffusion, surface interactions and boundary deformations. Even for relatively bigger length scales (up to 10 mm), effects like surface tension become significant. In this review article, we focus primarily on the study of deformable boundaries in small-scale flows.

The geometry for a large chunk of small-scale fluid flow problems is microchannels and pipes. A major effect deformable boundaries has on microchannel flows is significant reduction in pressure drop for the same flow rate as opposed to rigid microchannels[27]. The study of this pressure drop is crucial for accurate microchannel design, bioflow modelling[32, 43] and appropriate modelling of microchannel based applications (Secomb et al.[69]). Furthermore, deformation of channel walls could be used for flow control[98] in small-scale flow setups. On the other hand, flow through deformable pipes has largely been studied with the intent of understanding peristaltic flows[16], which is a pervasive mechanism in biological systems. Modelling of effects like trapping, entrainment and transport of bolus[38], which could be a blob of the fluid itself (e.g. mucus, blood) or a particle/body embedded in the fluid (e.g. RBC, administered drug, food bolus) present interesting and compelling problems. Furthermore, modelling of complex fluid and coupled phenomenon are also called for to have a better representation of associated bio-systems[8].

Another geometry ubiquitous in problems of the type considered in this article are two solid moving objects (typically, a sphere/cylinder and a plane) at small separation with intervening fluid. Such geometry is observed frequently in body joints, force-measuring instruments, etc. where the presence of a fluid assists in reducing wear as well as friction (see[33]). Study of structure deformation in such setups becomes a requirement to assess the load-bearing capacity and load response characteristics. The presence of other effects (e.g. electrokinetics) also need to be accounted for (see[91]). Such geometry has been

Department of Mechanical Engineering, IIT Kharagpur, Kharagpur, India.
**jeevan@mech.iitkgp.ernet.in*

Springer IISc Press

found in cell adhesion as well (see[94]), flow of lipid vesicles close to walls, car wipers and tyres on wet roads. Furthermore, an in-depth modelling and experimental analysis of sphere-near-deformable-substrate systems with intervening fluid has recently paved way for a contactless solid property characterization methodology proposed by Restagno et al.[63] and Carpentier et al.[13].

Another class of geometry is those involving thin solids (membranes, elastic sheets, vesicles). Use of membrane-based microchannels for building microfluidic circuits has been an emerging field in recent years[93], with flow being switched on and off by membrane deformation. Other uses of membrane-based microchannels is as pressure sensors[74]. The elastohydrodyamics of lubricated thin elastic sheets is another geometry that is gaining traction. The surface wake (which has been thoroughly studied in marine science) presents an opportunity for rheological studies at small-scale flows[44] and lubricated sheet is one of the prospective geometric setups for the same. Also, adhesion of lubricated sheet is a critical phenomenon for intercellular signalling[9] and wafer bonding[64]. Liquid splashing and spreading on membranes is another geometry of interest and is widely observed in nature, posing a rich field of study. For example, splashing of drops onto leaves can lead to damage and spread of foliar disease[25, 29], and splashing is considered an unwanted phenomenon in agricultural/industrial applications such as pesticide delivery, inkjet printing and spray coating[50, 83]; spreading of fluid on a thin elastic substrate occurs in neonatal respiratory distress syndrome[31].

This review article presents a broad overview of the contemporary research being conducted on small-scale flows with deformable boundaries. Given forth are four sections based on the geometry (except the fourth section, which covers associated works) of the system being studied, followed by the conclusion as the last section.

2 Channels and Tubes

Much of the research work corresponding to microfluidics has to do with microchannels, and the coupling of the channel wall deformations with the fluid flow poses an interesting problem and reveals some fascinating physics. Another geometry studied vividly is deformable tubes, where although there are some differences from microchannels (tubes have thin walls while microchannels typically have thick walls), they fall under the same broad category. With this view, this section starts with the seminal work by Gervais et al.[27] that has served as a starting point or a validation criterion for much of related subsequent works, the recent experimental exploration by Raj et al.[61], as well as the recent mathematical intensive pressure-drop modelling by Christov et al.[19], all three of which attempt to improve upon the understanding of fundamentals of the physical phenomenon involved, with major emphasis on pressure drop in deformable microchannels. They are followed by exposition of works by DelGiudice et al.[21] (experimental) and Meng and Thouless[52] (semi-empirical), who studied microchannel deformation as a requirement for microrheometry and crack propagation, respectively. Next, the work by Mukherjee et al.[54] is presented; they studied the influence of the presence of electrolytic species in the fluid on the wall deformation dynamics. Then, we present the work by Ismagilov et al.[36] also, who attempted to peruse the deformability of microchannels for device design to obtain mixing. Shifting our attention to tubes, pioneering work by Takagi and Balmforth[81] is presented, who studied peristaltic flow in deformable tubes. Subsequently, works by Takagi and Balmforth[80] and de Loubens et al.[49] are presented, where systems consisting of a solid object present in the fluid bulk being subjected to peristalsis are studied. Then, work by Goswami et al.[30] is presented, where the effects of complex fluid and electrokinetics on flow in deformable tube was explored. We close the section by touching upon the works by Kang et al.[41], de Rutte et al.[66] and Davies et al.[20], who worked on deformable microchannels, and Bandopadhyay et al.[5], Tripathi et al.[84], Beg and Tripathi[7] and Mukherjee and Shadden[53], who incorporated coupled physical effects in flow through deformable tubes.

Gervais et al.[27] studied the deformation of PDMS microchannels under imposed flow rates. Numerical solutions were attempted rather than analytical, as it was argued that none of the available analytical models accurately represent the problem. Scaling analysis was carried out as per the small displacement approximation. It was conjectured that vertical and horizontal displacements are of the order of $\frac{pw}{E_y}$ and $\frac{ph}{E_y}$, respectively, where p is pressure in the channel, h is the height and w is the width of the channel and E_y is the Young's modulus of the channel material. Hence, it could be deduced that for a channel that has width much higher compared to height, the horizontal (along width) deformation will be negligible compared to the vertical (along height) deformation. Further analysis revealed the proportionality constant connecting channel height

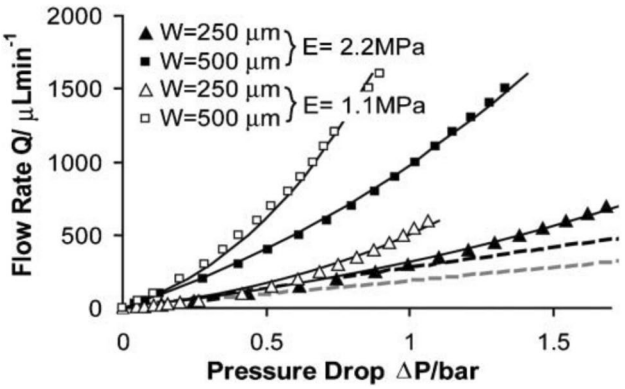

Figure 1: *Q* vs. Δ*P*—dashed lines: expected flow rate in the absence of channel deformation; solid lines: fit of obtained analytical expression to data (Re numbers varied from 0 to 100). Reproduced from Gervais et al.[27] with permission of The Royal Society of Chemistry.

increment with $\frac{pw}{E_y}$ to be of the order of unity. An important finding of the analysis was that the volume flow rate varies with the fourth power of pressure. The average fluid velocity was seen to increase towards the channel outlet (since the channel cross section decreases, but the volume flow rate remains the same). It was conjectured that this acceleration of flow could potentially cause an error in predicting quantities like shear stress in materials (e.g. PDMS). The trend of volume flow rate with pressure drop is presented (see Fig. 1). Thus, it was deduced that deformable channels need less pressure for the same flow rate than rigid walls.

Raj et al.[61] studied deformable rectangular cross-sectional microchannels using three approaches—pressure drop correlations, wall deformation correlations and micro-PIV-based experiments. The channel walls were approximated as thick plates, and a non-dimensional deformation parameter, α, was determined using scaling principles, whose value is fixed for a given geometry[18,27] and is calculable through fluid structure computations. A combination of equations, comprising empirical pressure drop expressions (dependent on flow rate and channel dimensions), expression of average deformed height[27], were obtained that lead to a flow-rate pressure-drop relation as well as a flow-rate deflection-profile relation, each of which was numerically solved for the given flow rates. It was established that α scales as ξ^3 (validated with experimental observations, where, $\xi = w/t$ is the width-to-thickness ratio of the channel). From the results, pressure drop was seen to have an almost linear (eventually saturating in experiments) variation with flow rate, with higher values for the non-deformable case; a good match with the thick-plate assumption model was found. Pressure drop was found to be as high as 28 percent even for a practically rigid substrate at high flow rate (since deformation, however small, does kick in). On the other hand, for a deformable microchannel, deformation was seen to be 0.95 times the undeformed channel height near the inlet and 0.4 times the undeformed channel height near the outlet, at high flow rates.

Christov et al.[19] also studied the relation between flow rate and pressure drop for shallow deformable microfluidic channels. Deformation was modelled using the steady-state displacement relation as per the Kirchhoff–Love equation. Subsequent mathematical analysis of the system showed a relation between the flow rate and pressure distribution (non-dimensional), which is akin to the relation established by Gervais et al.[27]. The obtained equation indicates that the flow rate is proportional to the cube of the channel height (thus, channel height deformation has substantial effect on pressure drop). As opposed to Gervais et al.[27], whose method needed a fitting parameter that has to be obtained for each channel shape by experimentation, this work presented a perturbation method-based solution for the flow rate to pressure drop relation using established mathematical frameworks (viz. Stokes equation obtained by lubrication approximation and theory of quasi-static isotropic bending of plate). However, this analysis did confirm that the flow rate is a quadratic polynomial of pressure drop as proposed by Gervais et al.[27]. Furthermore, it was brought to the fore that a highly nonlinear relation of pressure drop with flow rate for higher values of both has been reported in experiments.

DelGiudice et al.[21] explored the effect of channel deformation on microrheometry.

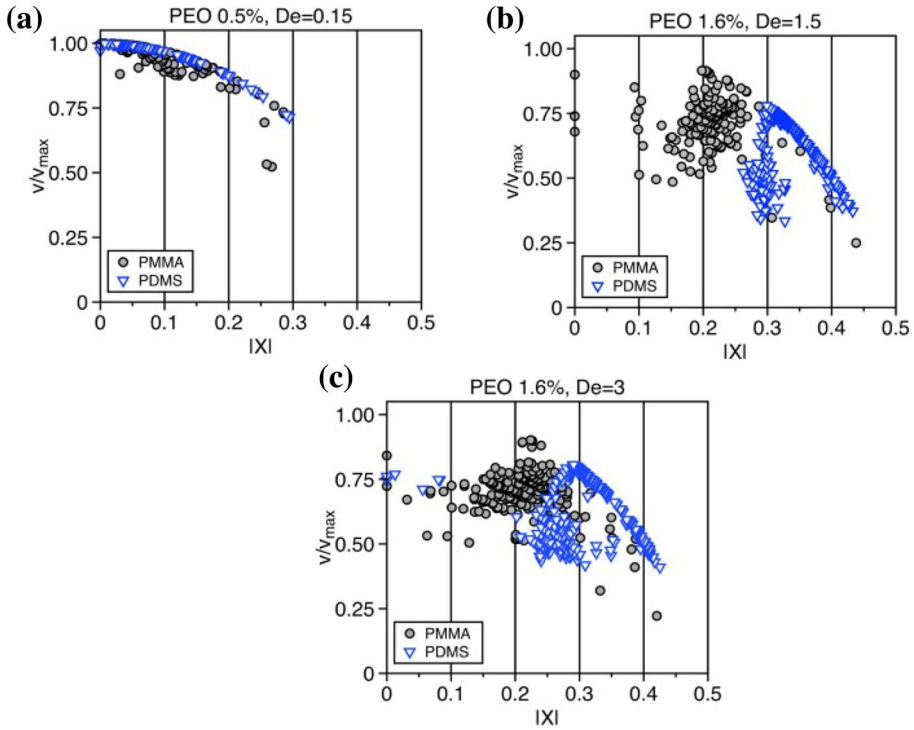

Figure 2: Normalized particle velocity as a function of the dimensionless coordinate $|X|$ for particles in both PMMA and PDMS systems for **a** PEO 0.5 % at De = 0.15 %, **b** PEO 1.6 % at De = 1.5 and **c** PEO 1.6 % at De = 3. Reprinted from DelGiudice et al.[21], with the permission of AIP Publishing.

Experiments with PDMS (polydimethyl siloxane, which is deformable) and PMMA (polymethyl methacrylate, which is three orders of magnitude stiffer and, hence, effectively rigid) were carried out and the significance of wall rigidity on particle migration characteristics was examined. The fluid used was PEO (polyethylene oxide) solution in water, which is weakly shear thinning to Newtonian. It was observed that the system with PDMS demonstrated a higher tendency of the particles to migrate towards the periphery than a system with PMMA, an effect that was seen to be exacerbated for higher concentration solutions (having higher Deborah numbers (De)) (see Fig. 2). The observations suggested that the measure of fluid relaxation time (which is the key measurement for microrheometry) would be unaffected by the channel material, provided the flow satisfies a low-De condition.

Meng and Thouless[52] studied (semi-analytically) the collapse and expansion of liquid-filled elastic cracks and channels. Analytical solutions were obtained for the axisymmetric cases (i.e. cylindrical channels) and elliptical channels of arbitrary aspect ratios. The governing equations and corresponding boundary conditions yielded a diffusion equation for radius of inner surface dependent on time and position along the axis (all three variables being normalized). It was found that the collapse of crack (estimated as location where dimension of cross section has shrunk by 50%) is expected to propagate as the square root of time and is smaller for higher aspect ratios.

Mukherjee et al.[54] studied the relaxation characteristics of a deformable microscale channel subjected to electro-osmotic flow. The geometry used was similar to that of Dendukuri et al.[22]. A skewness of the bulge due to electro-osmotic flow (which enhances one side's squeeze flow but inhibits the other side's, with the sides depending upon the sign of the zeta potential) was observed, which stands in contrast to the symmetric profile in the absence of EOF (see Fig. 3). It was concluded that the effective squeezing flow is not only qualitatively, but also quantitatively different because of the presence of EOF and the ratio of Debye length to half of the channel height determines the extent of the effects of EOF. Furthermore, the initial configuration of the channel wall has significant effects on the relaxation characteristics as well.

Ismagilov et al.[36] analysed an elastomeric microfluidic switch that can be used to control

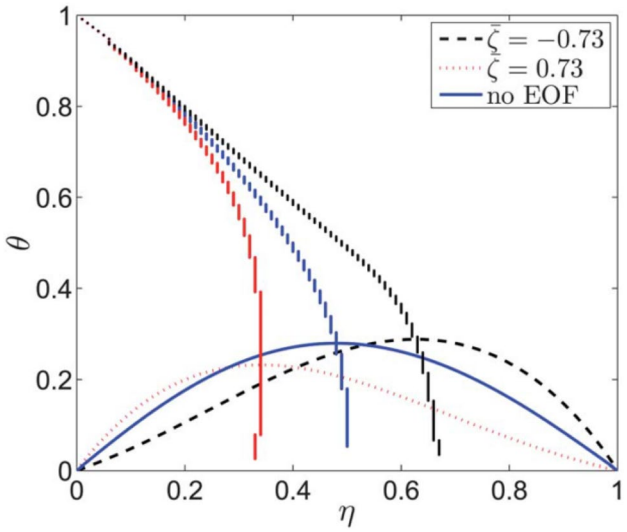

Figure 3: Asymmetric relaxation at change to non-dimensionalized time $\tau = 0.25$, corresponding to change to non-dimensionalized zeta-potential, $\bar{\zeta} = -0.73$ and $\bar{\zeta} = 0.73$; the results of $\bar{\zeta} = -0.73$ and $\bar{\zeta} = 0.73$ interchange perfectly when direction of the applied electric field is reversed (time-lapse snapshots of maximum points of the bulge corresponding to the squeeze flow also presented). Reproduced from Mukherjee et al.[54] with permission of The Royal Society of Chemistry.

flow between two tangentially perpendicular channel, one on top of the other with a square section common to the wall of the two. Two methods were explored, altering channel aspect ratio by pressure manipulation, or altering lateral position of a phase in a stream by injection of additional fluid. The advantage of elastomer-based microfluidic systems in offering the opportunity to alter the geometry of the system in real time (as opposed to rigid microfluidic systems that can only pre-actively be designed to have a particular geometry) was stipulated. Intuitive scaling analysis suggested that the height to width aspect ratio comes strongly into play in determination of the exchange rate. In the limiting case of small aspect ratio, the ratio of flow split was seen to follow the same correlation as pressure gradients (aspect ratio squared). Experimental characterization of flow split with aspect ratio and Reynolds number was thus established as the basis for quantitative control of the system.

A pioneering work on peristalsis was done by Shapiro et al.[70] , who studied the mechanics of low-Reynolds-number long-wavelength peristaltic pumping. They studied the case of infinite train of peristaltic waves and experimental validation was done as well, establishing reflux and trapping as major phenomenon of interest for peristaltic flows. In recent times, Takagi[81], studied the deformation of an elastic tube, thus causing peristaltic wave propagation, where both solitary and wave trains were considered. Pumping efficacy (defined as the ratio of net fluid flux to power input) was obtained and was observed to be highest for the case of a solitary wave of large amplitude (as opposed to wave trains or small-amplitude solitary waves). For small-amplitude forcing, asymptotic solution was obtained and matched well with for small η (where $\eta = \hat{\eta}R/\mu c$ is the forcing strength non-dimensional parameter, μ is the fluid's dynamic viscosity and $F(\hat{z} - ct) = \hat{\eta} f[(\hat{z} - ct)/L]$ is the external radial forcing, with $\hat{\eta}$ being the characteristic strength, L being the characteristic axial scale, c being the propulsion speed and f being a dimensionless function). On the other hand, corresponding to $\eta \gg 1$, for the case of periodic wave, q (a constant proportional to the volumetric flow rate) approached unity, i.e. full transport of the fluid was seen to occur with the wave, and two regions appeared in the flow domain, a narrow swollen blister near $z = 3\pi/2$ and a substantial occlusion for the remainder (i.e. $z > 3\pi/2$) of the tube (z is the non-dimensionalized z-coordinate, given as $z = \hat{z} - ct/L$) (see Fig. 4). For solitary waves, expansion waves were observed to create a translating inflated blister with radius of the order of η/D, where $D = \hat{D}R^3/\mu cL$ is the dimensionless stiffness.

As a development to their work already presented, Takagi[80] mathematically modelled the propulsion of a suspended, movable, slender,

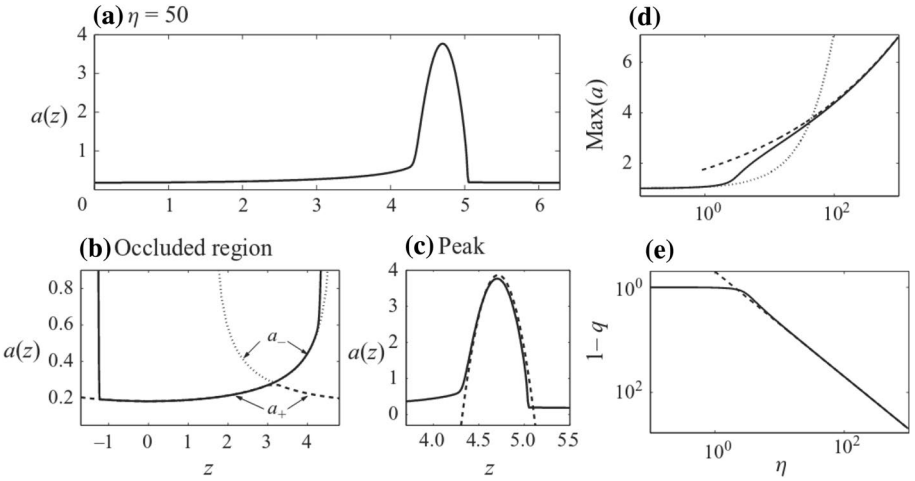

Figure 4: **a** Large-amplitude periodic wave magnifications of the occluded and blistered regions shown in (**b**) and (**c**), along with comparison to the asymptotic solutions for $a \approx a_{\pm}(z)$ (dashed and dotted lines in **b**), and the large-amplitude approximation (dashed line in **c**); **d**, **e** maximum wave amplitude (a_{max}) and flow deficit (1-q) against η (the dotted and dashed lines show the low-amplitude and large-amplitude predictions, respectively). Reproduced from Takagi and Balmforth[81] with permission from Cambridge University Press.

non-deformable body in an axisymmetric tube filled with fluid and subjected to peristalsis. The force balance associated with the object in the fluid determines the acceleration of the body. The cases that were considered were—solitary wave and periodic waves each with an infinite cylindrical rod and a parabolic finite lozenge. It was observed that for the infinite rod, periodic waves lead to profiles substantially similar to the case without the rod. Also, although a solitary wave is never able to generate enough traction to actuate motion of the rod, periodic wave trains can propel it at a slower-than-wave finite speed. As for the case of finite lozenges, propulsion by solitary waves was observed to be possible and it was established that there was a crossover forcing amplitude, above which the waves are strong enough to trap the object in the wave (a limited finite displacement was observed below the threshold).

de Loubens et al.[49] developed an elastohydrodynamic model of swallowing with Newtonian liquids and pharyngeal peristaltic wave with the purpose of understanding the effect of bolus and saliva viscosity on the kinetics of flavour release. Prediction of aroma release kinetics was attempted and the bolus movement was modelled as a forward roll coating process with deformability of mucosa taken into account. Limiting cases were distinguished (as also done by Johnson[39]) for high elasticity parameter (ratio of viscous force to elastic force) and low load parameter (ratio of external load to elastic forces), where viscous forces dominate and rigid roll limit is achieved, and for low elasticity parameter and high load parameter, elastic forces dominate and dry contact limit (large deflection) is achieved.

Goswami et al.[30] studied the peristaltic flow of a power law fluid through a nano-sized deformable tube, with effects of electrokinetics considered. Two regions in the fluid bulk were considered—the core, where power law behaviour was considered, and the periphery, where Newtonian behaviour was considered. Electrokinetics was incorporated by using the Helmholtz–Smoluchowski slip velocity rather than having an electrokinetic body force term in the momentum conservation equation. It was observed that the dependence of the interface between the two fluids on the viscosity ratio (which is dependent on the power law index) and on electro-osmotic slip velocity is analogous. An important result they arrived at was that the trapping of fluid bolus can be eliminated and the reflux can be reduced (both of which are characteristic of peristaltic flows) due to electro-osmosis-induced slip velocity, which decreases the resistance of the peristaltic wave against the momentum of the advancing fluid. On similar lines, it was stated that increasing the thickness of a less resistive peripheral region fluid (than core fluid) can remove trapping as well.

Kang et al.[41] studied (theoretically and experimentally) the deformation properties for periodic

circular obstacles in PDMS microchannels subject to flow using finite element analysis. de Rutte et al.[66] presented a numerical model to predict wall deformation in electrokinetically operated micro and nano channels. Davies et al.[20] did an experimental study of motion of rigid microbeads in shear flow near a wall, coated with a thin layer of soft polymer brush, a system akin to blood circulation. Contribution of cell and wall deformations to lubrication forces were found to be of comparable magnitude at sub-μm distances from wall. It was observed that gap height (between the beads and the wall) increased with flow strength.

Bandopadhyay et al.[5] did a similar study of electrolyte flow in a peristaltic channel (both periodic and single wave considered) in the presence of electro-osmosis-induced body force. Tripathi et al.[84] studied the flow of a viscoelastic fluid employing the Maxwell model through a peristaltic tube, where sinusoidal peristaltic waves were imparted to the tube wall. Beg and Tripathi[7] incorporated the effects of thermal as well as mass diffusion in nanofluid flow through a deformable tube being subjected to peristaltic pumping. Mukherjee and Shadden[53] studied the inertial particle dynamics in large artery flows. Soft-contact model was observed to come into play for negligible deformations for a particle suspended in flow. It was found that as the immersed particle comes close to a wall, a lubrication layer develops, thereby increasing the pressure on the particle and hence deforming it.

3 Objects Near a Wall

The geometry considered in this section is that of a large object (typically sphere or cylinder) near a wall. This geometry represents a distinct difference from the geometries in the previous sections because the fluid in the squeeze gap is directly exposed to a bulk. Up ahead, works by Restagno et al.[63], Steinberger et al.[75], Leroy et al.[46], Villey et al.[90] and Carpentier et al.[13] are elucidated, who have all studied squeeze flow interactions in the context of modelling mechanical behaviour through force and separation measurement techniques without hard contact. It is followed by fundamental works by Leroy and Charlaix[45], Snoeijer et al., Leroy and Charlaix[73] and Urzay[87]. Then, the fundamental works by Salez and Mahadevan[68], Urzay et al.[67] and Rallabandi et al.[62] are presented, followed by a thorough exposition of the study by Pandey et al.[57]. Subsequently presented are the works of Wang et al.[92] (where squeeze flow with compliant coating, modelled as a Kelvin–Voigt solid on rigid substrate, is studied), Wong[96] and Chakraborty[14], who have studied the effects of the presence of electrolytic species in the fluid being subjected to squeeze flow. Then, the works of Polychronopoulos and Papathanasiou[59], Stupkiewikz[77], Chakraborty and Chakraborty[15] and Naik et al.[55] who have studied coupled phenomenon (porosity, cavitation, electrokinetics and finite size effect of ions, respectively) with the fluid structure interactions, are presented. The section ends with the mentions of Balmforth et al.[3], Masjedi and Khonsari[51] and Tan et al.[82].

Restagno et al.[63] proposed the design and functioning of a surface force apparatus (SFA) meant to measure the forces of interaction between two solid surfaces (typically, a sphere near a plane). For the design proposed, the cantilever deflection was measured with a differential interferometer and a capacitive sensor was used to measure the separation between the ends of the two cantilevers. The cantilever displacement and its derivatives would be related to the force $F_s(h)$ acting between the surfaces as per the equation,

$$M\ddot{x} = -\lambda\dot{x} - Kx + F_s(h) + \delta f, \tag{1}$$

where $\dot{x}$ and $\ddot{x}$ are the first and second time derivatives of x ($x = x_{dc} - x_0$ is the displacement of the cantilever, with x_{dc} being the averaged value of x obtained from the optic and capacitive sensors, and x_0 is an unknown shift), M, λ and K are the mass, damping and stiffness parameters for the mass–damping–spring system modelled, $F_S(h)$ is the force acting between the surfaces and δf is the sum of other forces acting on the cantilever, the major contributors being capacity plate interactions and vibrations.

It was noted that the displacement is the combination of a slow monotonous approach or recession of surfaces and a small harmonic displacement. For the mathematical modelling, all the pertinent variables of the system (force, separation and displacement) were represented with complex notation as:

$$\begin{aligned} F_S(t) &= F_S(h(t)) = \hat{F}_S e^{j\omega t}, \\ h_{ac}(t) &= \hat{h}e^{j\omega t} \ , \ x_{ac}(t) = \hat{x}e^{j\omega t}, \end{aligned} \tag{2}$$

with the corresponding complex variables (i.e. $\hat{F}$, $\hat{h}$ and $\hat{x}$) giving their respective amplitudes as well as relative phases.

Hence, the relation between the three complex variables is established as

$$\frac{\hat{F}_S}{\hat{h}} = \frac{\hat{x}}{\hat{h}}(K + j\omega\lambda - M\omega^2) - \frac{\hat{\delta f}}{\hat{h}}, \tag{3}$$

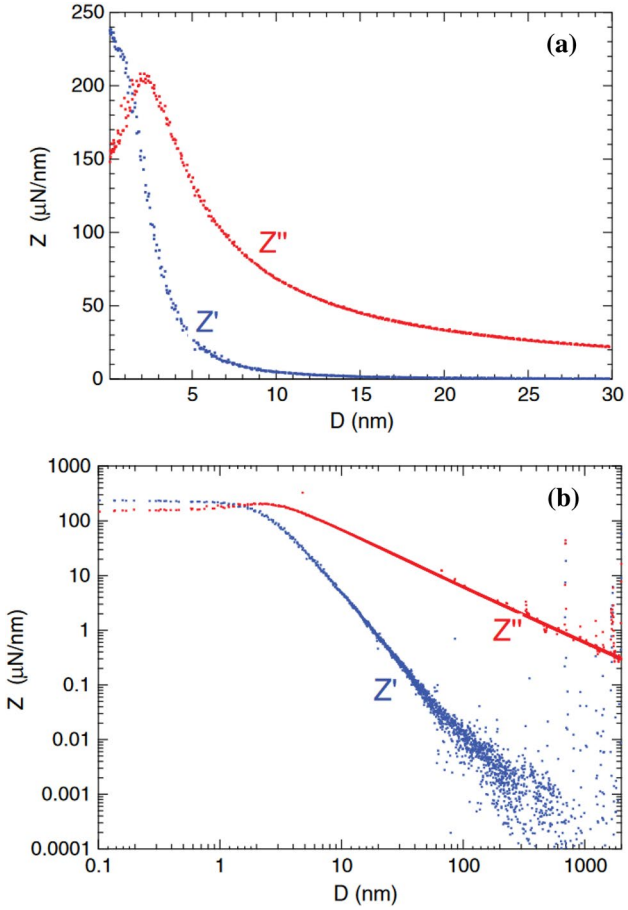

Figure 5: Damping (red points) and stiffness (blue points) measured with a water–glycerol mixture of viscosity 24.9 mPa-s, in **a** linear scale and **b** log–log scale; the frequency is $\omega/2\varpi = 19$ Hz, and the radius of the sphere is R=3.59 mm. Reprinted figure with permission from Villey et al.[90] Copyright (2013) by the American Physical Society.

where $\hat{F}/\hat{h}$ is called the transfer function and $\hat{\delta f}$ is the amplitude of δf. Therefore, the measurements of forces, amplitudes and cantilever displacements with time complete the system and make any further analysis possible. Of particular interest is the fact that the transfer function is expected to follow the relation obtained from lubrication theory

$$\frac{\hat{F}}{\hat{h}} = -\frac{j6\pi\eta R^2}{h}, \tag{4}$$

where η is the fluid viscosity, and R is the sphere radius.

Steinberger et al.[75] studied the elastic properties of a super-hydrophobic surface to obtain a model for surface elasticity measurement without contact using a liquid film as probe. Experiments with a thick elastic substrate were performed and it was demonstrated that reduction of viscous friction is wrongly attributed to slip rather than elastohydrodynamics. Furthermore, the elastic properties of a matrix of microscaled bubbles was determined from their free surface deformation.

Leroy et al.[46] studied the hydrodynamic interaction between an elastic planar substrate and a sphere at nanoscale using a dynamic SFA. For the SFA, the sphere was taken to be oscillating with an amplitude h_0 and frequency $\omega/2\pi$ above a surface. The dynamic response (i.e. ratio of force to separation), denoted by $\tilde{G}_\omega(D) = G'_\omega(D) + jG''_\omega(D)$, was dominated by viscous damping at large separations, with the viscous response component being $G''_\omega = 6\pi\eta\omega R^2/D$ and the deformability of the elastomer (associated with the real component, $G'_\omega(D)$) scaling as $1/D^{5/2}$ (where η is the bulk viscosity of the fluid, R is the sphere radius and D is the separation). At smaller separations, the two components were seen to become comparable and the damping no longer diverged as D^{-1}, because the fluid no longer gets expelled and the entire displacement of the sphere gets

accommodated by the deformation of the substrate. Therefore, it was established that at large separations, fluid probe acts like a dash pot of damping coefficient $\lambda(D) = 6\pi\eta R^2/D$, while at smaller separations, the fluid trapped in a central region acts like a solid probe. A crossover distance $D_k = 8R(\eta\omega/E^*)^{2/3}$ was identified for transition between the two regimes observed ($E^* = E/(1-\nu^2)$ is the reduced Young's modulus of the elastomer, where E is the Young's modulus and ν is the Poisson's ratio). Subsequently, experimentation with a thin incompressible film of substrate (approx. 5 μm) on a rigid platform was also performed. Although it was observed that the force response had a viscous-dominated regime at large separations (that saturates at small separations), much like for the thicker layer, the response was much stiffer and, hence, the elastic real part was always lower than the viscous dissipative part, decaying as D^{-4}. Mathematical formulation provided for this case was seen to match well with the experimental results.

Villey et al.[90] studied how surface elasticity affects the rheology on nanometric liquids. With the setup similar to Leroy et al.[46], it was shown that the elastic deformation of the two surfaces must be accounted for during assessment of the rheology of nanometric liquids. At large separations, the real part of impedance (ratio of force to separation) was seen to have tolerably vanished and the imaginary part was seen to vary as D^{-1} (D being the separation), similar to Leroy et al.[46]; for intermediate separations, a finite stiffness (real part of impedance) was observed, and below a critical threshold D_c (approx. 2 nm), the stiffness exceeded damping, indicating the beginning of the second regime (see Fig. 5, showing hydrodynamic impedance for a Newtonian intervening fluid).

Carpentier et al.[13] studied the dynamic force response of a sphere-plane geometry for a wide frequency range of sphere oscillation, where a static force was applied to the tip employing a force-feedback method. Sub-nanometer oscillations were added to the tip (i.e. the sphere) and a force feedback microscope (FFM) was used to measure the static force, and the dissipative and elastic parts of the interaction with a single AFM probe. Comparisons with an SFA having a two orders of magnitude bigger probe radius were done to establish the FFM as a nano-SFA. The theoretical modelling of dissipative and elastic part of force response were obtained similar to Leroy et al.[46]. It was concluded that the satisfactory extraction of the dynamic component of force response (validated using comparisons with SFA) strengthens the suitability of FFM as a candidate for measurement of mechanical properties of soft matter with intervening fluid setups, as well as their response to increase in frequency range.

Leroy and Charlaix[45] performed an in-depth mathematical study of small-amplitude oscillations of a sphere near a deformable wall with intervening fluid. A parabolic approximation of sphere surface was considered and a standard form of axisymmetric cylindrical co-ordinate Reynolds equation was used. After the requisite formulation, the cases of very thin compressible, very thin incompressible and very thick (approaching semi-infinite) elastic layer were considered (with a rigid platform below). As a result, scaling laws for force response (ratio of force to separation) were established, thereby enabling determination of elastic modulus of the substrate layer. At large separations, elastic force response was seen to decrease with -2.5 power of separation for semi-infinite layer, with -3 power for thin-compressible layer and -4 power for thin incompressible layer, whereas viscous response scaled with inverse of separation for all three cases. In contrast, for small separation, both elastic and viscous response saturated, but while elastic response remained smaller than viscous response for thin incompressible layer and equated viscous response for thin compressible layer, it overtook for semi-infinite layer.

Snoeijer et al.[73] studied the lubricated contact between two elastic bodies approaching each other at a relative speed U, considering substantial elastic deformation. It was brought to attention that opposed to the small deformation problems that can be solved using a perturbation approach, large deformation problems result in flat contact area (as in a Hertzian contact) with a thin lubrication layer whose thickness at the edge is described by an integro-differential equation, with solution as a non-local version of Bretherton's problem[10]. The entire system was seen to convert into a similarity equations problem using Hilbert transformation, which was solved numerically. Using the universal similarity solution along the upstream inlet, the thickness of the fluid film between the bodies was seen to scale as $U^{3/5}$.

Urzay et al.[87] did a mathematical study of the elastohydrodynamic force on a translating and rotating sphere close to a soft wall. The flow was modelled using Reynolds equation (and associated velocity expressions) by evoking lubrication approximation for the intervening fluid. Subsequently, perturbation approach was

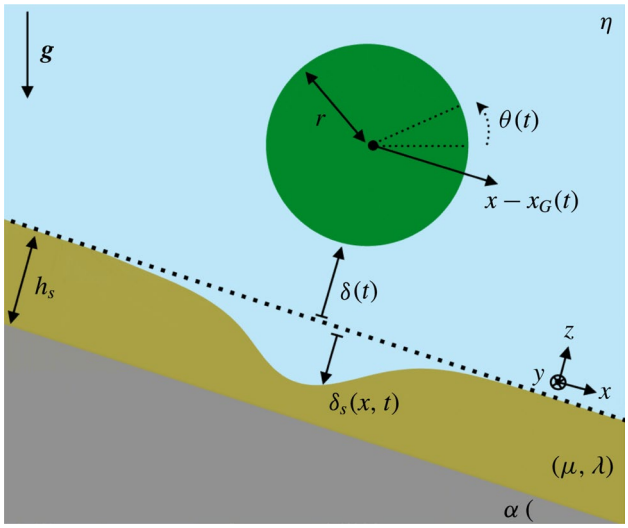

Figure 6: System schematic: a negatively buoyant cylinder (green) falling down under the influence of gravity , inside a viscous fluid (blue), in the vicinity of a thin soft wall (brown), with the ensemble lying atop a tilted infinitely rigid support (grey). Reproduced from Salez and Mahadevan[68] with permission of Cambridge University Press.

employed to solve Reynolds equation with the wall deformation accounted for, the perturbation parameter being the ratio of characteristic wall deformation to the smallest separation of sphere from undeformed wall. On similar lines, the wall deformation was solved for considering a thin compressible elastic layer, which enabled the use of perturbation approach using ratio of gel thickness to characteristic lubrication region dimension as the small parameter. As a further development of this work, Urzay[86] studied the effects of van der Waals forces and electrical double layer forces on the interaction between the sphere and the wall, using a similar perturbation approach. Furthermore, the sphere's adhesion and lift-off were studied and the effects of substrate thickness and incompressibility were considered.

Salez and Mahadevan[68] performed a theoretical study of elastohydrodynamics of sliding, spinning and sedimentation of a cylinder in proximity of a compliant wall (see Fig. 6). Scaling arguments were formulated that established regimes of sliding. Three degrees of freedom were established (which are functions of time)—gap between cylinder and undeformed wall, tangential coordinate of cylinder centre and angle of rotation of the cylinder. Parabolic profile of deformed interface and hence total gap profile was considered based on the Hertzian contact model[40], where elastic response is linearly related to pressure as elucidated by Skotheim and Mahadevan[71,72]. Scaling analysis based on balancing of lift force as per pressure expression of elastohydrodynamic theory (soft substrate effects) with gravity gave an expression for scaling of the equilibrium sliding height (δ_{eq}) at a given speed as

$$\delta_{eq} \sim \left(\frac{h_S \eta^2 \dot{x}_G^2}{\mu \sqrt{r} \rho^\star g \cos(\alpha)} \right)^{2/7}, \qquad (5)$$

where h_S is $-(2\mu + \lambda)\delta_S(x,t)/p(x,t)$ which is a constant, $\delta_S(x,t)$ is the deformation of the plane, μ and λ are Lamé parameters, $p(r, t)$ is the local pressure, η is the fluid viscosity, $\dot{x}_G$ is the x-component of the cylinder velocity, α is the angle of incline of the plane, $\rho^\star$ is the cylinder's density, r is the cylinder's radius, g is the acceleration due to gravity and the $x - y - z$ co-ordinate system is as presented in Fig. 6.

Analysis of a small perturbation about the equilibrium sliding height suggested that the cylinder will oscillate with frequency of the order of $\left(\frac{\rho^\star g \cos(\alpha)}{\rho \delta_{eq}}\right)^{0.5}$, which will decay over a time period of the order of $\left(\frac{\delta_{eq}}{r}\right)^{1.5} \frac{m}{\eta}$ (ρ is density of the fluid, and m is mass of the cylinder). If initiated with a spin, a Magnus-like effect was observed (i.e. cylinder lifts off from wall whilst still sliding) due to rotation-induced shear leading to increased hydrodynamic pressure and hence normal force.

Saintyves et al.[67] did an experimental study of self-sustained lift of a cylinder close to a soft wall and the low friction between them, occurring

because of soft lubrication. A negatively buoyant cylinder immersed in a fluid and moving parallel to and close to a soft-coated inclined wall was studied. A self-sustained lift was seen to be induced, leading to a reduction in the friction by almost an order of magnitude. A simple scaling principle was developed that validated the experimental results. Over a wide range of parameters, steady sliding of the cylinder was observed, with the asymmetric elastic oil interface deformation leading to the self-sustained lift. It was asserted that since elliptical cylinders, which do not rotate, show similar dynamics, rolling can be ruled out as leading to lift force. Through theoretical analysis corresponding to modified lubrication approximation accounting for soft substrate, and small strain approximation for substrate deformation, scaling of lift force was obtained as $\frac{\eta^2 V^2 R^{1.5} h}{G\delta^{3.5}}$, where η is the fluid viscosity, V is the sliding speed, R is the cylinder radius, h is the soft-coating thickness, G is the shear modulus and δ is the minimum undeformed gap. The obtained results started deviating from expectation for very soft substrates, because, arguably, strain started becoming nonlinear.

Rallabandi et al.[62] studied the rotation of a cylinder immersed in a fluid and sliding near a thin elastic coating on a rigid platform. Stokes flow was considered, and elastic deformation was considered to be proportional to the normal stress (Winkler approximation). It was shown that in the lubrication limit, an infinite cylinder translating with constant speed and separation parallel to a soft wall, must also rotate to be torque free. Based on scaling assumptions typical of lubrication approximation and aforementioned approximation of deformation, a dimensionless elastic compliance Λ (i.e. ratio of characteristic deformation to lubrication gap) was identified. A translating cylinder was shown to have no torque up to the leading order in Λ, but higher order torque contributions could not be ruled out as the formulation indicated. Lorentz reciprocal theorem was used, and angular velocity of cylinder was shown to scale with the cube of sliding speed. Torque per unit length thus obtained was seen to scale with Λ^2 (in contrast to leading order lift force that scales with Λ).

Pandey et al.[57] studied the lubrication of soft contacts, with solids being treated as viscoelastic. The geometry considered was cylinder close to a soft plane with intervening fluid. Three models were considered—Kelvin–Voigt, standard linear solid and power law rheology. Four cases were considered—rotating rigid cylinder near a soft wall, rotating soft cylinder near a rigid wall (c.w. rotational speed ω), translating rigid cylinder near a soft wall and translating soft cylinder near a rigid wall (horizontal speed V). For the formulation, lubrication pressure was treated as an incompressible stress acting on the semi-infinite viscoelastic solid. It is noteworthy that the interface stress formulation used for this work, that is for a semi-infinite solid, stands in contrast with that by Skotheim and Mahadevan[71,72], who studied elastic layer of finite thickness on a rigid platform. Subsequent mathematical analysis brought forth the non-dimensional parameter β (ratio of characteristic elastic deformation to typical gap size) which was used as small parameter for perturbation expansion of Reynolds equation. For further analysis, pressure's timescale, l / V (ratio of characteristic contact length $l = \sqrt{2\Delta R}$ to cylinder velocity, with R being the cylinder radius, Δ being the minimum undeformed separation between the cylinder and the plane) was denoted as τ_p; relaxation time of the viscoelastic wall was denoted by τ; and the ratio of τ to τ_P, which is a key parameter in determining the system's response (analogous to Deborah number, and zero for case of purely elastic solid), was denoted as $\mathscr{T}$. For the SLS model, it was also observed that for increasing τ, deformation decreases and symmetry breaking occurs, but as τ approaches infinity, instaneous response occurs, and symmetry is re-established but with a scale reduction of $(1+c)^{-1}$, where c is the ratio of the two spring stiffnesses. Turning our attention to the KV model, it was seen to become purely elastic for very small values of ω and behave like Newtonian fluid for very large values of ω. Finally, for the power law model, it was seen that for small values of $\mathscr{T}$, lift force is similar to that of the elastic case, but for large values of $\mathscr{T}$, L/L_0 scales as $|\mathscr{T}|^{-n}$ (n is the exponent in power law formulation); furthermore, there is a sudden change from $\mathscr{T}^{-n}$ to $\mathscr{T}^{-2}$ for large τ as n approaches unity. It was thus asserted that all models could be conformed to the arbitrary form of $\mu(\omega) = G'(\omega) + iG''(\omega)$, where G' is the storage modulus and G'' is the loss modulus.

Wang et al.[92] studied (theoretically and experimentally) the out-of-contact elastohydrodynamic deformation of an elastic film subjected to drainage flow due to lubrication forces. The motion considered was the perpendicular approach of a rigid sphere towards a surface with a compliant coating. Dimple formation for the thick film case was found to occur and prevent contact, whereas for the thin film case, full contact was seen to be reached. It was posited that for thin films, the underlying substrate can counter

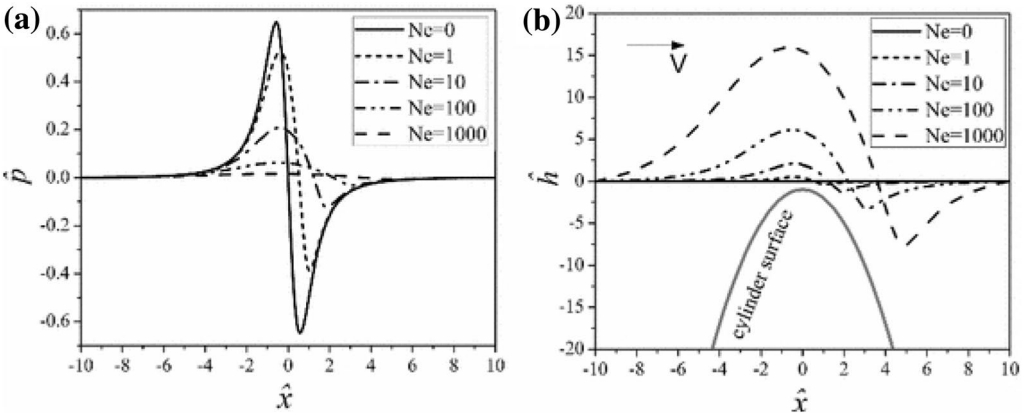

Figure 7: **a** Dimensionless pressure (non-dimensionalized with $ph_0^2/\mu\ Vl$) and **b** dimensionless gap for different values of *Ne* and $\hat{K} = 0$; the impermeable flexible web is assumed to move with velocity *V* to the right. Reprinted by permission from Springer Customer Service Centre GmbH: Springer Nature Transport in Porous Media[59].

significant fraction of the mechanical stresses, which alters its elastohydrodynamic response compared to semi-infinite solids. Furthermore, given dimple formation was occurring, dimple growth occurred with a barrier ring that followed the same geometric scaling as for fluid droplets and that was independent of the material properties (radius of barrier ring: $r_b = (0.5RVt_d)^{0.5}$, where R and V are radius of the spherical probe and approach velocity, respectively, and t_d is the time since start of dimple formation). As the force increased, the contact area of indentation increased, while the elastohydrodynamic pressure distribution became sharper and more concentrated near the centre.

Wong et al.[96] studied the effects of electric double layer on the dynamics of very thin lubricating films. Both rigid and elastic substrates were considered. Modified Reynolds equation as per Zhang and Umehara[99] was used to obtain the effective viscosity. Semi-empirical equations by Dowson[23] were used to incorporate elastohydrodynamics. It was found that presence of an electric double layer substantially increases the thickness of the lubricating film. However, the effects were found to be significant only for separations up to 100 *nm* and were high for rigid wall, but negligible for elastic wall. It was also found that the effective viscosity increases with square of zeta potential and decreases with the cube of separation.

Chakraborty and Chakraborty[14] studied the influence of electrical double layer and the associated streaming potential on the elastohydrodynamics of a compliant substrate being dynamically loaded with a spherical probe at a small separation. The system consisted of an oscillating hard spherical probe at a small separation from an elastic substrate with an intervening electrolytic solution. Complex formulation for the pertinent variables, similar to Steinberger et al.[75], was used. The system was considered to be quasi-static as far as electrokinetics is concerned and a closed-form piecewise expression of electric potential was obtained. The substrate deformation was considered to be linearly related to the local pressure as per $\xi(r,t) = K^{-1}P(r,t)$, where $\xi(r,t)$ is the local deformation, K is the stiffness per area of the elastic substrate and $P(r, t)$ is the local pressure. The results thus obtained indicated an increasing force response with α (ratio of minimum undeformed separation to probe radius), growing higher for higher zeta potential and for lower κ ($\kappa = H/\lambda$, where $H(r, t)$ is the height of the spherical probe from the undeformed substrate, lambda is Debye length, epsilon is the fluid's permittivity, n_0 is the electrolyte number density in the electroneutral bulk and $\bar{y}$ is the dimensionless distance along the y-axis that is non-dimensionalized with $H(r, t)$).

Polychronopoulos and Papathanasiou[59] studied the mechanics of fluid penetration in a soft permeable web layer moving past a static rigid cylinder. The fluid flow was taken to be defined by lubrication theory and fluid transfer through web layer by Darcy's law. Based on the findings of Yin and Kumar[97], the web–liquid interface deformation was taken to be linearly proportional to the local gap pressure (similar to cases of membranes). Therefore, fluid penetration was found to be dependent upon elasticity (represented by the dimensionless parameter *Ne*, ratio of viscous

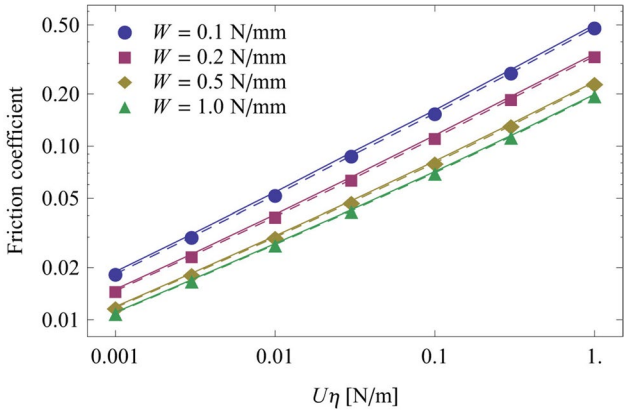

Figure 8: Friction coefficient as a function of $U\eta$; dashed lines correspond to the appropriately modified Couette shear stress. Reprinted from Stupkiewicz et al.[77], with permission from Elsevier.

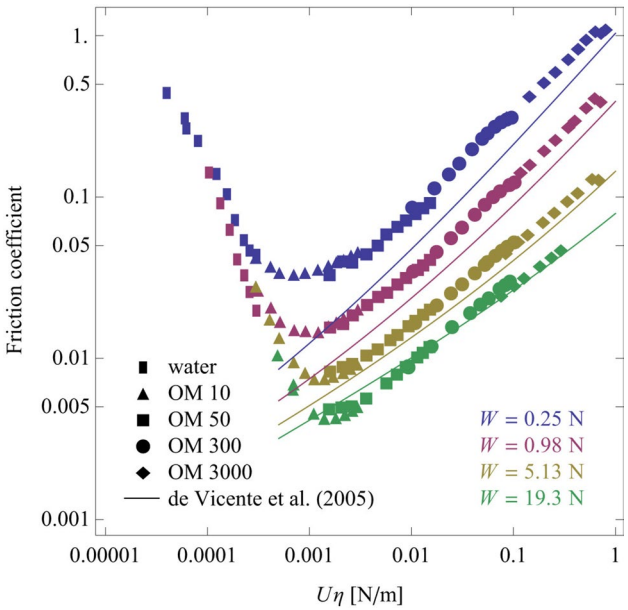

Figure 9: Friction coefficient as a function of $U\eta$ for five lubricants and a range of loads W; solid lines indicate the predictions of the regression equation of de Vicente et al.[89]. Reprinted from Stupkiewicz et al.[77], with permission from Elsevier.

force to elastic force) and permeability (represented by the dimensionless parameter $\hat{K}$) and a specific combination was found to exist for maximum penetration depth. The web permeability, K, was taken to vary as $K = K_{ref} - \beta\, p$ (K_{ref}, being the reference permeability, and β being the permeability's sensitivity to pressure, and p being the fluid pressure). Equations were then non-dimensionalized as per norms of lubrication theory and expressions for the two parameters Ne and $\hat{K}$ were identified as $Ne = \frac{\mu V H l}{E h_0^3}$ and $\hat{K} = \frac{K l^2}{h_0^3}$, where μ is the fluid viscosity, H is the undeformed web thickness, $l = \sqrt{2Rh_0}$ is the characteristic lubrication dimension, V is the web's sliding speed, R is the cylinder radius, h_0 is the minimum undeformed web–cylinder separation and E is the web's Young's modulus. It was observed that as one proceeds from zero value of Ne to higher, pressure starts deviating from an anti-symmetric solution and the gap loses its symmetric form (see Fig. 7). From the solutions, it could be seen that lift increases, reaches a maxima and then decreases against Ne, the reason for which was suggested as being the competition

between symmetry breaking and lowering pressure. As a contrast, for the case of rigid permeable web, it was seen that the pressure decreases and the liquid interface (front of the fluid penetration) increases with increasing permeability; however, both remain symmetric rather than losing symmetry. Furthermore, it was observed that the penetration is small for very deformable as well as rigid webs, but variation in $\hat{K}$ causes large effects on penetration for intermediate elasticities. Lastly, solution by perturbation approach with *Ne* as the small parameter was obtained and was found to have a good match with the numerical solutions (better for smaller $\hat{K}$).

Stupkiewicz et al.[77] studied the finite deformation effects in soft elastohydrodynamic lubrication problems, which are typically neglected in classic elastohydrodynamic lubrication theory. The geometry considered was a rigid cylinder near an elastic substrate. Reynolds equation, finite strain elasticity equations and Elrod–Adams-like model for cavitation were used for modelling. A rigid cylinder subjected to a vertically downward loading (with W as the loading per unit length) and sliding against a soft elastic layer with harder thin upper coating and a rigid platform underneath was considered first and the results obtained were reported (see Fig. 8, where U is called the entrainment speed, which is half of the sliding speed, and η is the fluid viscosity). It was observed that friction coefficient is a function of $U\eta$ and load and the form of the function is practically identical to that for linear elasticity model; however, the film thickness and pressure profiles were quite different, with the linear model underestimating the film thickness. Experimental validation was also performed along with the numerical method wherein a tribometer for high load was designed with an elastomeric ball on a rotating disk, and plots of friction coefficient against $U\eta$ were obtained (see Fig. 9). It is to be noted that for higher values of $U\eta$, friction coefficient varies linearly on the log–log plot (as expected for hydrodynamic lubrication regime), but at low $U\eta$, linearity is not found.

Chakraborty and Chakraborty[15] studied the influence of electrolytic species for a planar slider bearing (an inclined plane moving right at speed U above a flat plane, with separation of h_1 at left end, h_2 at right end and horizontal length L) with intervening fluid containing a symmetric electrolyte. The variation of load capacity per unit width (integral of pressure with length) (denoted by W) against ratio of h_2 to h_1 (denoted by r) was presented, which was seen to be increasing, reaching a maxima and then decreasing for compliant substrate while monotonously decreasing for stiff substrate. Naik et al.[55] studied the finite size effects of ionic species on compliant surface flow dynamics. Geometry similar to Chakraborty and Chakraborty[15] was used. Stokes equation with electric field as body force, and Poisson–Boltzmann equation were considered as the governing equations for the system. Steric effects, which influence ionic distribution profile as well as diffusivities of cations and anions (diffusivity is obtained from the Nernst–Einstien relation and interplay of Stokes drag with electric force), were incorporated into the system. Charge-induced thickening[6] was used to account for changed dynamic viscosity due to charged species being present in the fluid, leading to the expression for dynamic viscosity (μ),

$$\frac{1}{\mu} = \frac{1}{\mu_0}\left(1 - \frac{1}{2}\nu\left|\frac{n_+ - n_-}{n_0}\right|\right), \tag{6}$$

where, μ_0 is the reference dynamic viscosity (i.e. dynamic viscosity of the bulk fluid not considering any charge-induced thickening), n_0 is the number density of the cations and anions in the electroneutral bulk, n_+ and n_- are the local number densities of cation and anion, respectively, and ν is the steric factor which accounts for the finite size effects of the ions. Pressure was taken to balance the y-normal stress at interface and dependence of y-normal stress on x and z deformations was done away with by invoking the lubrication approximation, yielding the expression for deformation as $s_y = -h_l p/(\lambda + 2G)$, where s_y is the deformation along the y-axis (axis perpendicular to the deformable plane), h_l is the thickness of the compliant substrate (which rests on a rigid support), λ and G are the Lameé parameters and p is the local pressure.

Balmforth et al.[3] studied the effects of solid elasticity and fluid compressibility on the gravity-caused sinking of a two-dimensional (infinitely long along the third dimension) smooth rigid object towards a plane wall (an elastic plane coating on a rigid base) through a viscous fluid (with pressure-dependent viscosity), where asymptotic and numerical solutions were obtained to study the final approach to contact. Masjedi and Khonsari[51] studied line-contact elastohydrodynamic lubrication of soft materials. Based on simulations, expressions were obtained to estimate the film thickness and load. Behaviour of Stribeck curves was used to study variations of the traction coefficient. Reynolds equation was altered to be for mixed elastohydrodynamic lubrication as given by Patir and Cheng[58]; since the pressure is low, the problem had been treated as isoviscous. Subsequent analysis of the problem showed that

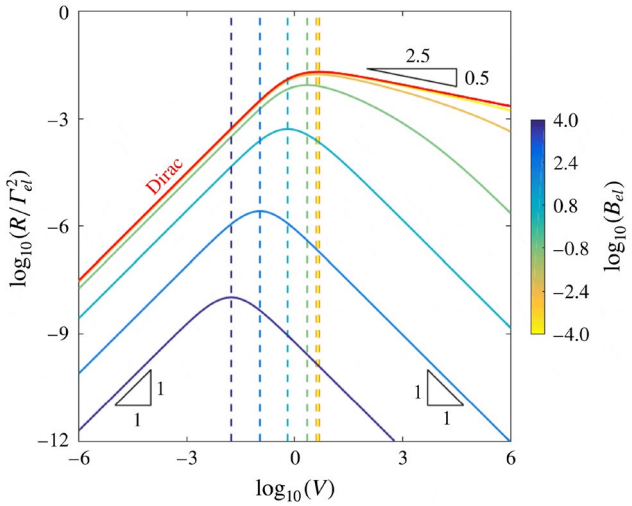

Figure 10: Normalized wave resistance as a function of the reduced speed, for various elastic Bond numbers B_{el}; the Dirac limit ($B_{el} \to 0$) is indicated; the vertical dashed lines indicate the position of the maximal wave resistance, for each value of B_{el} Reproduced from Arutkin et al.[1] with permission of Cambridge University Press.

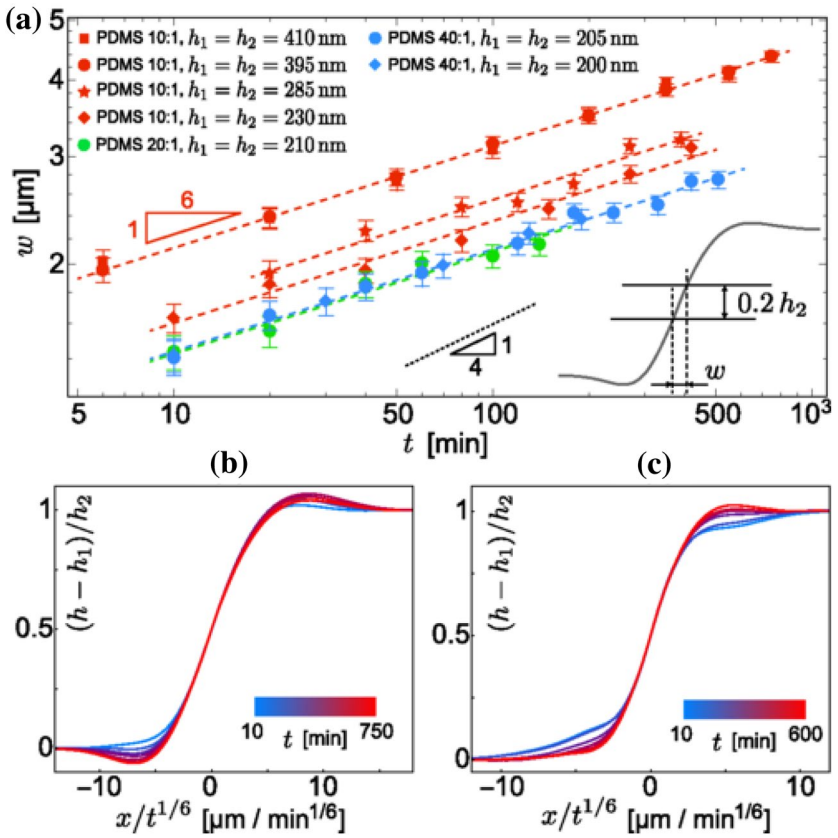

Figure 11: **a** Experimental evolution of the profile width w (proportional to the lateral extent of the linear region as displayed in the inset) as a function of time t, in log–log scale, for samples involving different liquid-film thicknesses and substrate elasticities; all datasets appear to have a $t^{1/6}$ power relation. The slope corresponding to a $t^{1/4}$ evolution (rigid-substrate case) is displayed for comparison; **b** Experimental levelling profiles on 10:1 PDMS with the horizontal axis scaled by $t^{1/6}$ (c) Experimental levelling profiles on 40:1 PDMS with the horizontal axis scaled by $t^{1/6}$. Reprinted figure with permission from Rivetti et al.[65] Copyright (2017) by the American Physical Society

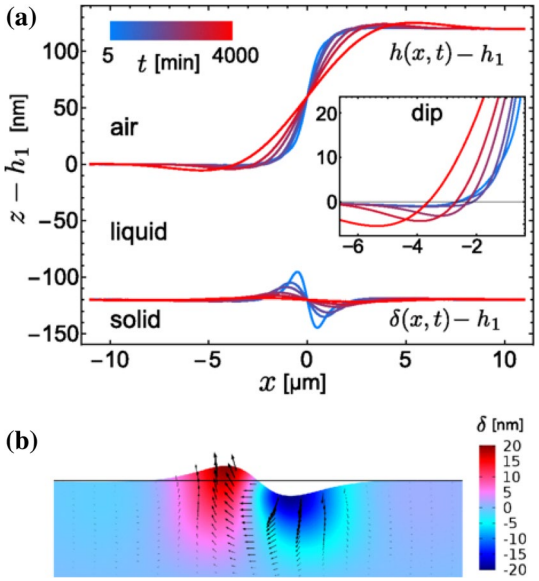

Figure 12: **a** Theoretical profiles for the liquid–air interface $z = h(x,t)$ and the solid–liquid interface $z = \delta(x,t)$, both shifted vertically by $-h_1$ (with s_0 (elastic layer thickness) = 2 m, $h_1 = h_2 = 2h_0/3 = 120$ nm, μ (elastic layer's Young's modulus) = 25 kPa, $\gamma = 30$ mN/m, $\eta = 2.5$ MPa-s); inset displays a close-up of the dip region; **b** finite element simulation (COMSOL) of solid's total displacement (black arrows) and its vertical component δ (colour coded) (result obtained by imposing the Laplace pressure field corresponding to the first profile in **a** to a slab of elastic material exhibiting comparable geometrical and mechanical properties, and maximal displacement of 22 nm found in good agreement with theoretical prediction shown in (**a**). Reprinted figure with permission from Rivetti et al.[65] Copyright (2017) by the American Physical Society.

for the considered problem, isoviscous solution can be used, with asperity radius and surface roughness being the influential parameters. Tan et al.[82] studied the dynamic behaviour of wax-in-oil flow at the contact between a rigid glass plate sliding below a stationary polyurethane elastomeric sphere, where the behaviour of entrapped wax particles was found to depend on the soft lubrication observed.

4 Thin and Free Geometries (Membranes, Beams, Sheets, Films and Vesicles)

The flow of work presented in this section follows. We first present the works of Carlson and Mahadevan[12] and Arutkin et al.[1], who have studied flexible sheets near rigid walls with intervening fluid; next are the works of Rivetti et al.[65] and Zheng et al.[100], who have studied flow over an elastic substrate or membrane with the other face exposed to air. Subsequently, work by Howell et al.[34, 35] is presented where flow over an elastic beam is studied. Then we present the works of Carlson and Mahadevan[60] and Arutkin et al.[17], who have all studied membrane attached to microchannels. The section ends with brief mentions of the work of Karpitschka et al.[42], who has modelled a typical physiological phenomenon involving deformable boundaries in microflows.

Carlson and Mahadevan[12] studied the dynamics of an elastic sheet close to adhesion to a wall with fluid in between. The effects of van der Waals adhesion potential was considered, leading to the transverse load balance as

$$\hat{p}(\hat{x},\hat{t}) = B\left.\frac{\partial^4 \hat{h}}{\partial \hat{x}^4}\right|_{(\hat{x},\hat{t})} + \frac{A}{3\hat{h}^3(\hat{x},\hat{t})}, \qquad (7)$$

where $\hat{p}$ is the local pressure, $\hat{x}$ is the x-coordinate, $\hat{t}$ is time, B is the bending stiffness, $\hat{h}$ is the height of the elastic sheet from the wall and A is the Hamaker's constant.

The standard Reynolds equation was arrived at with the pressure term as given in equation 7. Adopting the similarity conversion as $h(x,t) = (t_C - t)^{\alpha} H(\eta)$ (h, x, t are the dimensionless version of $\hat{h}$, $\hat{x}$, $\hat{t}$, respectively) with the similarity variable $\eta = \frac{x - x_C}{(t_C - t)^{\beta}}$ (α and β are arbitrary parameters, both being 1 / 3, t_C is the contact time, x_C is the contact point), an ordinary differential equation for the variable $H(\eta)$ was arrived at (whose solution includes a singularity as time approaches t_C). A simple power law

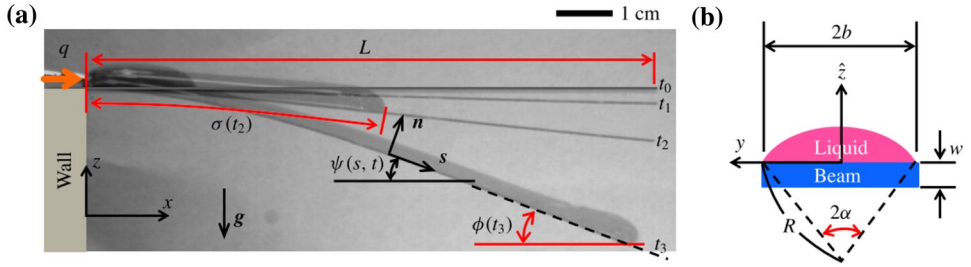

Figure 13: Experimental apparatus. **a** Side view (thin elastic beam of length L fixed at the left wall with constant flow rate q injected along the beam, wetted length denoted by σ (t), deflection angle at the advancing front by ϕ (t) and local deformation angle at arc length s by ψ (s,t), with time progressing as $t_0 < t_1 < t_2 < t_3$; **b** front view: cross-sectional shape of the liquid rivulet on the beam.

Reproduced from Howell et al.[35] with permission of Cambridge University Press.

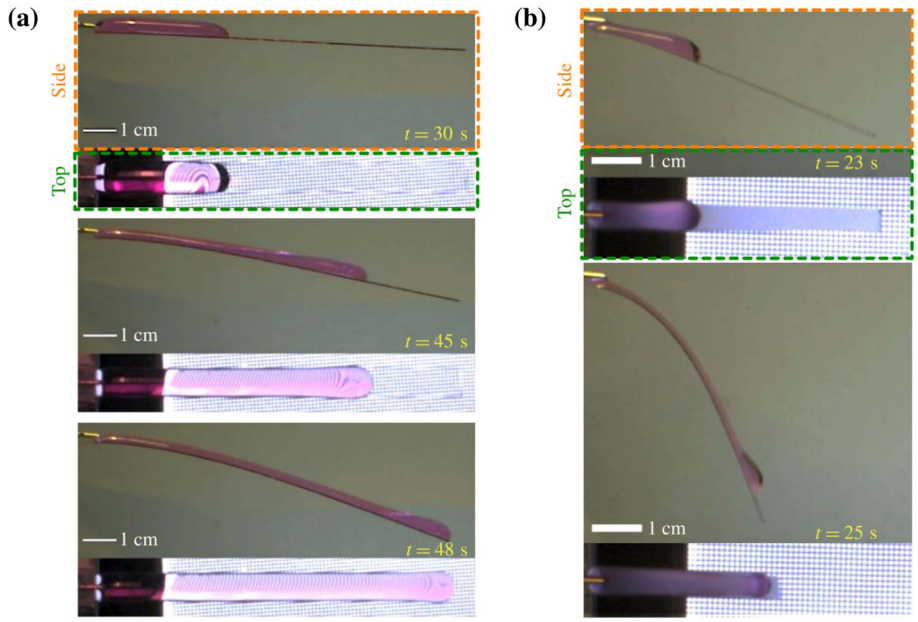

Figure 14: Side and top views of liquid flow over the elastic beam. **a** Small beam deflection case ($E = 2.4$ *GPa*, $q = 1.4 \times 10^8$ m^{3}s^{-1}, $L = 100$ mm, $w = 0.51$ mm, $2b = 7$ mm); **b** large beam deflection case ($E = 3.6$ GPa, $q = 2.2 \times 10^8$ m^{3}s^1, $L = 50$ mm, $w = 0.076$ mm, $2b = 4$ mm). Reproduced from Howell et al.[35] with permission of Cambridge University Press.

formulation between height and deformation was thus established, and the similarity analysis led to a self-similar shape for the elastic sheet as it approached touchdown.

Arutkin et al.[1] studied the elastohydrodynamics of a thin elastic sheet lubricated by a narrow liquid film and subjected to a moving pressure disturbance, with focus on the deformation wake and wave resistance. The externally applied pressure disturbance on the top elastic film was $\psi_{ext}(x - vt, y)$ (x and y being axes along the substrate's plane and v being the speed of motion of the externally applied pressure along x), which translated to an axisymmetric Lorentzian pressure field. It was found that the elastic Bond number appears as the key non-dimensional parameter given as $B_{el} = (a\kappa_{el})^2$, where a is the characteristic horizontal size of the external pressure field and $\kappa_{el} = \left(\frac{B}{\rho \cdot g}\right)^{(-1/4)}$ is the gravito-elastic length, with $B = \frac{Ed^3}{12(1-\nu^2)}$ being the bending stiffness, d the sheet thickness, E and ν the Young's modulus and Poisson ratio of the sheet respectively, ρ the fluid density and g the acceleration due to gravity. Low-speed and

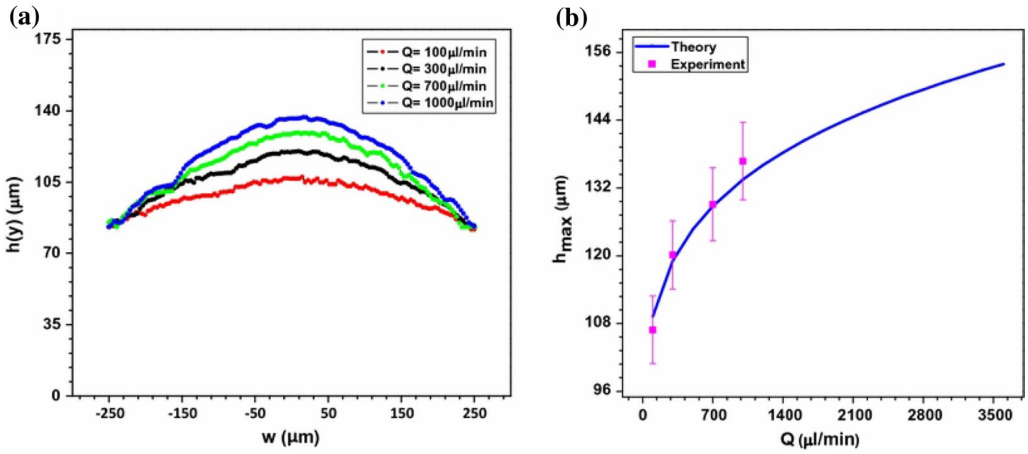

Figure 15: **a** Deflection height profile $h(y)$ of the membrane wall at various flow rates Q obtained using fluorescence imaging; **b** maximum deflection of the membrane wall h_{max} versus flow rate Q with comparison of model predictions with experimental data. Reprinted by permission from Springer Customer Service Centre GmbH: Springer Nature Microfluidics and Nanofluidics,[60].

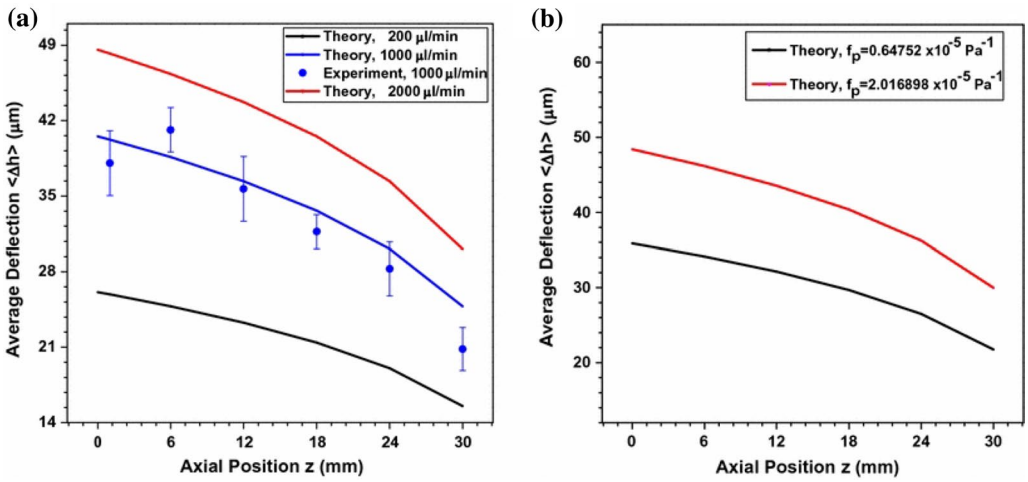

Figure 16: **a** Average axial deflection profile $\langle \Delta h \rangle$ of the membrane wall at various flow rates Q with f_p=1.0210^5 Pa_{-1} and comparison with experimental data; **b** average axial deflection profile $\langle \Delta h \rangle$ of the membrane wall at various compliance parameters f_p (w = 500 µm, h_0 = 83 µm, Q = 1000 µl/min). Reprinted by permission from Springer Customer Service Centre GmbH: Springer Nature Microfluidics and Nanofluidics[60].

high-speed regimes were taken up to obtain analytical asymptotic solutions, considering a thin layer. It was observed that for small velocities, there was no wake and only a symmetric disturbance occurred, but for large velocities there was a wake behind (i.e. dipped interface) and an accumulation ahead (i.e. bumped interface). Larger elastic Bond number was seen to lead to a wider pressure field and hence lower wave resistance and vice versa (approaching the one associated with Dirac pressure field, i.e. $\hat{\Psi} = 1$, see Fig. 10).

Rivetti et al.[65] did the experimental study (AFM based) and theoretical modelling of a thin polymeric film on elastic substrate. The starting geometry is a stepped layer of fluid spread infinitely along the width as well as length, and height $h_1 + h_2$ right of the step. Mathematical solutions were obtained using Fourier transformations. Polystyrene (PS) was the material considered, since for the timescales of the experiment, it functions like a Newtonian viscous fluid. In the experimentation, it was observed that as the interface evolves, a dip and a bump appear and the depth of dip as well as height of bump eventually saturate (in contrast to rigid substrate case where the maximum and minimum

heights are entirely determined by starting heights and stay constant through evolution). It was inferred that the negative Laplace pressure underneath the dip pulls PDMS upwards and the opposite occurs for bump, and no-slip condition coupled with the flow induces a horizontal displacement field, causing deformations that subsequently affect the liquid–air interface due to the requirement of volume conservation. The definition of profile width considered was $w(t) = x(h = h_1 + 0.6h_2) - x(h = h_1 + 0.4h_2)$, and it was seen to scale as one-sixth power of time (see Fig. 11a). It was observed that scaling of profile width as one-sixth power of time accounts for most of the evolution for practical purposes. Profile width was expected to vary linearly with $\frac{\gamma h_0^3 t}{\eta}$, where t is time and $h_0 = h_1 + h_2/2$. Evolution of profile (both liquid–air and liquid–liquid) and the corresponding PDMS bulk deformation simulations are also presented (see Fig. 12). From the simulation results, for all viscosities, the profile was expected to approach the case of rigid substrate with time, starting farther off and taking longer for lower viscosity. However, this expectation was not fulfilled by experimental observations where the scaling was observed as one-sixth power of time rather than the one-fourth power of the rigid case. It was argued that the resulting curvature of the fluid–air interface that occurs as a result of translation of the fluid–solid interface due to volume conservation leads to a relatively lower Laplace pressure and, therefore, slowing down of the levelling process (leading to a smaller effective exponent).

Zheng et al.[100] studied the propagation of a thin fluid film over a thin elastic membrane, driven by buoyancy. The system is a coupled physical system comprising film thickness, membrane shape and radial tension within the film's region and membrane shape and radial tension outside. For small time, spreading of liquid and stretching of membrane were observed to be buoyancy controlled, liquid front evolution scaling with square-root of time, while for large time, membrane stretching caused the spreading and the system was found to be quasi-static (with a flat air–liquid interface), liquid front evolution scaling with the fourth root of time (edge effects come into effect further late in time). Laboratory experiments for constant fluid injection was done and good agreement with theoretical predictions was observed.

Howell et al.[34] studied the flow of a thin liquid film towards the free end on a flexible beam, considering gravity to be the dominant force. Mathematical modelling and non-dimensionalization similar to that by Howell et al.[35] was employed. It was observed that the fluid film thickness first increases and then decreases with the beam length, the reason being posited that the longer beam, suffering larger deflection, enhances the gravitational forcing on the fluid and, hence, exacerbates flow away from source. Howell et al.[35] expanded on their former work and validated their work with experimentation as well. Dynamics were found to fall into a small-deflection regime and a large-deflection regime and power laws for three time periods were established—the liquid just begins deforming the beam, beam deflection rises fast due to weight of the liquid film and the beam is bent to almost vertical. Studies were done with the flow rate of the fluid kept constant. The geometry of the problem statement is represented in Fig. 13 (flow rate of fluid kept constant), and the small deflection and large deflection regimes are represented in Fig. 14. For small deflection regime, deflection was seen to scale as four-fifth power of time for small time limit and fourth power of time for large time limit, and, maximum deflection angle was seen to scale as thirteen-fifth power of time for small time limit and ninth power of time to large time limit. For the large deflection regime, for up to intermediate time limits, similar behaviour as for small deflection regime was observed, but for large time limits, deflection was seen to scale linearly with time and maximum deflection angle approached $\pi/2$.

Raj and Sen[60] studied the flow-induced deformation of compliant membrane taken as the top surface of microchannels. Side walls and lower wall were semi-infinite and considered rigid. Using theoretical model as per Bruus[11], the expression for height as $h(z) = h_0(1 + (f_P p(z))^{1/3})$ (z being the axis along the channel) was considered. Pressure was observed to decrease linearly with axial position, increase linearly with fluid viscosity and decrease almost linearly with the compliance parameter. Linearly increasing pressure drop with flow rate for both rigid and compliant microchannels was observed with a faster slope for the rigid microchannel. The observed deformation was approximately parabolic (see Fig. 15). Average deflection was observed to decrease along the axial position (approximately linearly), with higher values for higher flow rate and for higher compliance parameter (see Fig. 16). The maximum deviation from experimental results was 18 %. Finally, pressure drop characteristics of compliant microchannel showed a 63 % lower pressure drop due to top wall deformability.

Cheikh & Lakkis[17] designed microfluidic transistors for amplification and flow control of lab-on-a-chip devices based on elastic membrane microchannels (that are pressure difference actuated). An improved modelling of single membrane microchannel was claimed that allows for more accurate estimation of pressure profile and membrane deflection. Modelling of the system analogous to DC electricity was done by equating pressure over flow rate to resistance, and hence MOSFET-like behaviour is modelled. It was deduced that for a single membrane, capacitor-like behaviour occurs when the membrane deflects away from channel and transistor-like behaviour occurs when the membrane deflects into the channel.

Karpitschka et al.[42] studied the dynamics of inward folding of a soft gel surface with a gel-based controlled-deformation setup. Mathematical analysis of the system revealed the cusp width to scale as 3/2 power of the distance from the tip. To demonstrate the suitability of mechanics of elasticity for mathematical modelling of such systems, a two-dimensional (plane strain) finite element simulation using the theory of finite deformations with an incompressible neo-Hookean constitutive equation was carried out. The same features as in the experiments (including the similarity collapse with the same universal shape superimposed) were obtained.

5 Associated Works

In this section, works related to flow-control devices that employ deformability of fluid–structure interfaces (i.e. valves, pumps, actuators, etc.) have been presented. The works in this section thus represent research that does not directly approach the problem of deformable boundaries in microconfined flow, but draw from it.

Flow actuation using deformable channels has been researched for a while now. One of the pioneering works in this field is by Unger et al.[85], who proposed an extension to soft lithography (named as multi-layer soft lithography) using soft materials that can be used to build active microfluidic systems with valves, switches and pumps made entirely out of elastomers.

Studer et al.[76] carried out the evaluation of scaling characteristics of low-pressure actuated microfluidic valves. Characterization was done by measuring actuation pressure and flow resistance (and subsequently compared to finite element simulations and alternative valve geometries). It was argued that although the aspect ratio of geometries for formerly reported works were required to be low, it is desirable to have unit aspect ratios in some applications. Two methods for flow actuation using pressure control were presented—push-down, where membrane thickness is dependent on geometry, and the device is like a stick-on on the substrate; and push-up where the membrane thickness is uniform and independent of the geometry of the device, and the device has to be fabricated with the substrate. For validation of the results with finite element modelling, the membrane material was considered to be a near-incompressible neo-Hookean solid. Subsequently, parametric studies were done to assess the effects of channel width and membrane thickness on the actuation pressure. It was found that push-up valves show an order of magnitude lower actuation pressure than push-down valves, which show hysteretic behaviour because of sticking of the membrane to the opposite wall.

Liu et al.[48] carried out experimentation, modelling and numerical simulation of the response characteristics of a microscale pneumatic actuator for microfluidic chips. For the same, PDMS elastomer was modelled as near-incompressible neo-Hookean material and plane-strain theory (large-deformation membrane behaviour theory) was employed. It was found that the maximum displacement of deflection was found to be proportional to one-third power of pressure difference across the membrane. Finite element simulation of the system was done and reasonable match between experimental, modelling and simulation results was demonstrated. A fourth-order fit of pressure offset to get the maximum deflection was obtained.

Gerasimenko et al.[26] performed modelling and characterization of a pneumatically actuated peristaltic micropump. The resistance of the channel was considered when calculating deflection of the membrane. Displacement of the membrane from quiescent position was described employing the dynamic equations of motion. PDMS was modelled using the Kelvin–Voigt model and the Young's modulus was considered to depend on the pressure over the membrane and other geometric parameters (centre deflection from quiescent position, design geometries, etc.) as

$$E = \frac{3}{16}\frac{R^4}{h^3}\left(1-\nu^2\right)\frac{p}{w_0}, \tag{8}$$

where E is the PDMS Young's modulus, R is the membrane radius, h is the thickness of

the membrane, ν is the Poisson's ratio, p is the pressure over the membrane and w_0 is the deflection of the membrane centre from its quiescent position. The membranes were actuated by air pressure in pneumatic tubes, and the time dependency of air pressure in pneumatic tubes was obtained from established governing equations. Shear deformations of membrane was not considered and analysis of membrane was done by representing it as a finite thickness of the film at the mid-plane. Semi-empirical solutions employing Bessel functions and Green's function were obtained.

Oh et al.[56] proposed an alternative and more effective (in terms of flow rate and valve efficiency) structural design of pneumatic valve (made of PDMS, whose deformability was employed for actuation) as opposed to the typical rectangular cross-sectional valves. The effectiveness of the proposed structure was elucidated with finite element analysis using COMSOL, employing the linear elastic model for PDMS.

6 Conclusion

In this review article, we have aimed to present an overview of contemporary research that involves fluid flow in small-scale geometries with deformable boundaries. There have been substantial amount of in-depth mathematical analyses of the associated phenomenon for different geometries as has been reported. It is noteworthy that although the standard linear elastic model and its derivatives and offshoots have been studied commonly, there has been no dearth of modelling the deformable boundaries (and underlying bulk if applicable) as viscoelastic solids[92, 57] as well as hyperelastic solids[42, 76]; furthermore, one study of finite deformation fluid–structure interactions has also been explored[77]. The most ubiquitously studied substrate was PDMS (owing to its suitability and ease of application for a vast expanse of research activities), and its modelling as a viscoelastic solid appeared to yield more appropriate results than as linear elastic. Although the fluid being studied was mostly Newtonian, there were noteworthy instances of non-Newtonian fluid being studied (shear-thinning fluid studied by Raj and Sen[60], Casson fluid by Vajraveluet al.[88], power law fluid by Goswami et al.[30] and pressure-dependent viscosity by Balmforth et al.[3]); furthermore, studies involving dispersion or dissolved species in fluid were also present (wax-in-oil by Tan et al.[82] and multiple instances of electrolytic solutions). There was a vast plethora of coupled physical phenomenon being modelled with the fluid–structure interactions as well, like contact line dynamics[65], electrokinetic effects[54], fluid mixing[36], bolus motion[80], van der Waals forces[12], porosity[59] and pneumatics[56]. All three approaches towards the problem (viz., analytical, numerical and experimental) have been substantially represented. There are instances of analytical approaches incorporating transforms—Hilbert[73] and Fourier[57, 65], exotic mathematical functions—Green's function[73], empirical expression-based methods[96, 60], scaling analyses[67, 28], asymptotics[34, 35] and similarity solutions[12, 100]. The primary choice for numerical solutions has been finite element analysis using available packages such as COMSOL and Abaqus. Experimental studies spanned those intended for physical studies, validation of mathematical/numerical results and design of devices. One major stream of work that stood apart was that by Restagno et al.[63], Leroy et al.[46], Villey et al.[90], Carpentier et al.[13] and Garcia et al.[24], which represents a steady approach towards understanding squeeze flow phenomenon to enable effective surface force measurements at a distance for material property determination.

Although a wide range of themes incorporating elasticity–flow interactions has been presented in this work, there is still a vast web of similar disciplines whose magnitudes would warrant a separate treatment and hence been deemed beyond the scope of this article. Examples include studies of fibre appendages protruding out of channel walls[47, 95], modelling of microswimmers[4, 2], flow through collapsible tubes[32, 37] and effects of surface tension and contact line dynamics on soft solids[78, 79].

Received: 20 March 2018 Accepted: 28 April 2018
Published online: 21 May 2018

References

1. Arutkin M, Ledesma-Alonso R, Salez T, Raphael E (2017) Elastohydrodynamic wake and wave resistance. J Fluid Mech 829:538–550
2. Avron JE, Kenneth O, Oaknin DH (2005) Pushmepullyou: an efficient micro-swimmer. New J Phys 7(1):234
3. Balmforth NJ, Cawthorn CJ, Craster RV (2010a) Contact in a viscous fluid. part 2. a compressible fluid and an elastic solid. J Fluid Mech 646:339–361
4. Balmforth NJ, Coombs D, Pachmann S (2010b) Microelastohydrodynamics of swimming organisms near solid boundaries in complex fluids. Quart J Mech Appl Math 63:267–294

5. Bandopadhyay A, Tripathi D, Chakraborty S (2016) Electroosmosis-modulated peristaltic transport in microfluidic channels. Phys Fluids 28(5):052002. https://doi.org/10.1063/1.4947115
6. Bazant MZ, Kilic MS, Storey BD, Ajdari A (2009) Towards an understanding of induced-charge electrokinetics at large applied voltages in concentrated solutions. Adv Colloid Interface Sci 152(1):48–88
7. Beg OA, Tripathi D (2011) Mathematica simulation of peristaltic pumping with double-diffusive convection in nanofluids: a bio-nano-engineering model. Proc Inst Mech Eng Part N J Nanoeng Nanosyst 225(3):99–114
8. Bohme G, Muller A (2013) Analysis of non-newtonian effects in peristaltic pumping. J Nonnewton Fluid Mech 201:107–119
9. Bongrand P (2018) Physical basis of cell-cell adhesion. CRC Press, Boca Raton
10. Bretherton FP (1961) The motion of long bubbles in tubes. J Fluid Mech 10(2):166–188
11. Bruus H (2009) Theoretical microfluidic. Oxford University Press, Oxford
12. Carlson A, Mahadevan L (2016) Similarity and singularity in adhesive elastohydrodynamic touchdown. Phys Fluids 28(1):011702
13. Carpentier S, Rodrigues MS, Charlaix E, Chevrier J (2015) Proximity effect on hydrodynamic interaction between a sphere and a plane measured by force feedback microscopy at different frequencies. Appl Phys Lett 107(4):044101
14. Chakraborty J, Chakraborty S (2010) Influence of streaming potential on the elastic response of a compliant microfluidic substrate subjected to dynamic loading. Phys Fluids 22(12):122002. https://doi.org/10.1063/1.3524530
15. Chakraborty J, Chakraborty S (2011) Combined influence of streaming potential and substrate compliance on load capacity of a planar slider bearing. Phys Fluids 23(8):082004
16. Chakraborty S (2006) Augmentation of peristaltic microflows through electro-osmotic mechanisms. J Phys D Appl Phys 39(24):5356
17. Cheikh M, Lakkis I (2016) Microfluidic transistors for analog microflows amplification and control. Microfluidics Nanofluidics 20(6):91
18. Cheung P, Toda-Peters K, Shen AQ (2012) In situ pressure measurement within deformable rectangular polydimethylsiloxane microfluidic devices. Biomicrofluidics 6(2):026501
19. Christov I, Cognet V, Shidhore T, Stone H (2017) Flow rate–pressure drop relation for deformable shallow microfluidic channels. ArXiv e-prints
20. Davies H, Debarre D, Verdier C, Richter R, Bureau L (2017) Lift at a soft wall. ArXiv e-prints
21. DelGiudice F, Greco F, Netti PA, Maffettone PL (2016) Is microrheometry affected by channel deformation? Biomicrofluidics 10(4):043501
22. Dendukuri D, Gu SS, Pregibon DC, Hatton TA, Doyle PS (2007) Stop-flow lithography in a microfluidic device. Lab Chip 7:818–828
23. Dowson D (2012) Bio-tribology. Faraday Discuss 156:9–30
24. Garcia L, Barraud C, Picard C, Giraud J, Charlaix E, Cross B (2016) A micro-nano-rheometer for the mechanics of soft matter at interfaces. Rev Sci Instrum 87(11):113906
25. Gart S, Mates JE, Megaridis CM, Jung S (2015) Droplet impacting a cantilever: a leaf-raindrop system. Phys Rev Appl 3:044019
26. Gerasimenko T, Kindeeva O, Petrov V, Khaustov A, Trushkin E (2017) Modelling and characterization of a pneumatically actuated peristaltic micropump. Appl Math Model 52:590–602
27. Gervais T, El-Ali J, Gunther A, Jensen KF (2006) Flow-induced deformation of shallow microfluidic channels. Lab Chip 6(4):500–507
28. Gielen M, de Ruiter R, Snoeijer J, Gelderblom H (2017) Supressed splashing on elastic membranes. ArXiv e-prints
29. Gilet T, Bourouiba L (2015) Fluid fragmentation shapes rain-induced foliar disease transmission. J R Soc Interface 12(104):
30. Goswami P, Chakraborty J, Bandopadhyay A, Chakraborty S (2016) Electrokinetically modulated peristaltic transport of power-law fluids. Microvasc Res 103:41–54
31. Grotberg JB (2011) Respiratory fluid mechanics. Phys Fluids 23(2):021301
32. Grotberg JB, Jensen OE (2004) Biofluid mechanics in flexible tubes. Annu Rev Fluid Mech 36(1):121–147
33. Hamrock B, Schmid S, Jacobson B (2004) Fundamentals of fluid film lubrication. Taylor & Francis
34. Howell PD, Robinson J, Stone HA (2013) Gravity-driven thin-film flow on a flexible substrate. J Fluid Mech 732:190–213
35. Howell PD, Kim H, Popova MG, Stone HA (2016) Rivulet flow over a flexible beam. J Fluid Mech 796:285–305
36. Ismagilov RF, Rosmarin D, Kenis PJA, Chiu DT, Zhang W, Stone HA, Whitesides GM (2001) Pressure-driven laminar flow in tangential microchannels: G an elastomeric microfluidic switch. Anal Chem 73(19):4682–4687
37. Jensen OE (1990) Instabilities of flow in a collapsed tube. J Fluid Mech 220:623–659
38. Jiménez-Lozano J, Sen M, Dunn PF (2009) Particle motion in unsteady two-dimensional peristaltic flow with application to the ureter. Phys Rev E 79:041901

39. Johnson KL (1970) Regimes of elastohydrodynamic lubrication. J Mech Eng Sci 12(1):9–16
40. Johnson KL (1985) Contact mechanics. Cambridge University Press, Cambridge
41. Kang C, Overfelt RA, Roh C (2013) Deformation properties between fluid and periodic circular obstacles in polydimethylsiloxane microchannels: experimental and numerical investigations under various conditions. Biomicrofluidics 7(5):054102
42. Karpitschka S, Eggers J, Pandey A, Snoeijer JH (2017) Cusp-shaped elastic creases and furrows. Phys Rev Lett 119:198001
43. Kizilova N, Hamadiche M, el Hak MG (2012) Mathematical models of biofluid flows in compliant ducts. Arch Mech 64(1):65–94
44. Ledesma-Alonso R, Benzaquen M, Salez T, Raphael E (2016) Wake and wave resistance on viscous thin films. J Fluid Mech 792:829–849
45. Leroy S, Charlaix E (2011) Hydrodynamic interactions for the measurement of thin film elastic properties. J Fluid Mech 674:389–407
46. Leroy S, Steinberger A, Cottin-Bizonne C, Restagno F, Leger L, Charlaix E (2012) Hydrodynamic interaction between a spherical particle and an elastic surface: a gentle probe for soft thin films. Phys Rev Lett 108:264501
47. Lindstrom SB, Uesaka T (2007) Simulation of the motion of flexible fibers in viscous fluid flow. Phys Fluids 19(11):113307
48. Liu X, Li S, Bao G (2016) Numerical simulation on the response characteristics of a pneumatic microactuator for microfluidic chips. J Lab Autom 21(3):412–422
49. de Loubens C, Magnin A, Doyennette M, Trelea IC, Souchon I (2011) A biomechanical model of swallowing for understanding the influence of saliva and food bolus viscosity on flavor release. J Theor Biol 280(1):180–188
50. Lupoi R, O'Neill W (2010) Deposition of metallic coatings on polymer surfaces using cold spray. Surf Coat Technol 205(7):2167–2173
51. Masjedi M, Khonsari M (2017) Mixed lubrication of soft contacts: an engineering look. Proc Inst Mech Eng Part J J Eng Tribol 231(2):263–273
52. Meng F, Thouless MD (2017) The collapse and expansion of liquid-filled elastic channels and cracks. J Appl Mech 82:1–11
53. Mukherjee D, Shadden SC (2017) Inertial particle dynamics in large artery flows G implications for modeling arterial embolisms. J Biomech 52:155–164
54. Mukherjee U, Chakraborty J, Chakraborty S (2013) Relaxation characteristics of a compliant microfluidic channel under electroosmotic flow. Soft Matter 9:1562–1569
55. Naik KG, Chakraborty S, Chakraborty J (2017) Finite size effects of ionic species sensitively determine load bearing capacities of lubricated electrokinetics and surface compliance. Soft Matter 13:6422–6429
56. Oh CK, Lee SW, Jeong OC (2015) Fabrication of pneumatic valves with spherical dome-shape fluid chambers. Microfluid Nanofluid 19(5):1091–1099
57. Pandey A, Karpitschka S, Venner CH, Snoeijer JH (2016) Lubrication of soft viscoelastic solids. J Fluid Mech 799:433–447
58. Patir N, Cheng HS (1978) An average flow model for determining effects of three-dimensional roughness on partial hydrodynamic lubrication. J Lubr Technol 100:12–17
59. Polychronopoulos ND, Papathanasiou TD (2017) Fluid penetration in a deformable permeable web moving past a stationary rigid solid cylinder. Transp Porous Media 116(1):393–411
60. Raj A, Sen AK (2016) Flow-induced deformation of compliant microchannels and its effect on pressure-flow characteristics. Microfluidics Nanofluidics 20(2):31
61. Raj MK, DasGupta S, Chakraborty S (2017) Hydrodynamics in deformable microchannels. Microfluidics Nanofluidics 21(4):70
62. Rallabandi B, Saintyves B, Jules T, Salez T, Schonecker C, Mahadevan L, Stone HA (2017) Rotation of an immersed cylinder sliding near a thin elastic coating. Phys Rev Fluids 2:074102
63. Restagno F, Crassous J, Charlaix E, Cottin-Bizonne C, Monchanin M (2002) A new surface forces apparatus for nanorheology. Rev Sci Instrum 73(6):2292–2297
64. Rieutord F, Bataillou B, Moriceau H (2005) Dynamics of a bonding front. Phys Rev Lett 94:236101
65. Rivetti M, Bertin V, Salez T, Hui CY, Linne C, Arutkin M, Wu H, Raphaël E, Bäumchen O (2017) Elastocapillary levelling of thin viscous films on soft substrates. Phys Rev Fluids 2:094001
66. de Rutte JM, Janssen KGH, Tas NR, Eijkel JCT, Pennathur S (2016) Numerical investigation of micro- and nanochannel deformation due to discontinuous electroosmotic flow. Microfluidics Nanofluidics 20(11):150
67. Saintyves B, Jules T, Salez T, Mahadevan L (2016) Self-sustained lift and low friction via soft lubrication. Proc Nat Acad Sci 113(21):5847–5849
68. Salez T, Mahadevan L (2015) Elastohydrodynamics of a sliding, spinning and sedimenting cylinder near a soft wall. J Fluid Mech 779:181–196
69. Secomb TW, Hsu R, Pries AR (1998) A model for red blood cell motion in glycocalyx-lined capillaries. Am J Physiol Heart Circ Physiol 274(3):H1016–H1022
70. Shapiro AH, Jaffrin MY, Weinberg SL (1969) Peristaltic pumping with long wavelengths at low reynolds number. J Fluid Mech 37(4):799–825
71. Skotheim JM, Mahadevan L (2004) Soft lubrication. Phys Rev Lett 92:245509

72. Skotheim JM, Mahadevan L (2005) Soft lubrication: the elastohydrodynamics of nonconforming and conforming contacts. Phys Fluids 17(9):092101
73. Snoeijer JH, Eggers J, Venner CH (2013) Similarity theory of lubricated hertzian contacts. Phys Fluids 25(10):101705
74. Song W, Psaltis D (2011) Optofluidic membrane interferometer: an imaging method for measuring microfluidic pressure and flow rate simultaneously on a chip. Biomicrofluidics 5(4):044110
75. Steinberger A, Cottin-Bizonne C, Kleimann P, Charlaix E (2008) Nanoscale flow on a bubble mattress: effect of surface elasticity. Phys Rev Lett 100:134501
76. Studer V, Hang G, Pandolfi A, Ortiz M, Anderson WF, Quake SR (2004) Scaling properties of a low-actuation pressure microfluidic valve. J Appl Phys 95(1):393–398
77. Stupkiewicz S, Lengiewicz J, Sadowski P, Kucharski S (2016) Finite deformation effects in soft elastohydrodynamic lubrication problems. Tribol Int 93:511–522
78. Style RW, Boltyanskiy R, Che Y, Wettlaufer JS, Wilen LA, Dufresne ER (2013) Universal deformation of soft substrates near a contact line and the direct measurement of solid surface stresses. Phys Rev Lett 110:066103
79. Style RW, Jagota A, Hui CY, Dufresne ER (2017) Elastocapillarity: surface tension and the mechanics of soft solids. Ann Rev Condens Matter Phys 8(1):99–118
80. Takagi D, Balmforth NJ (2011a) Peristaltic pumping of rigid objects in an elastic tube. J Fluid Mech 672:219–244
81. Takagi D, Balmforth NJ (2011b) Peristaltic pumping of viscous fluid in an elastic tube. J Fluid Mech 672:196–218
82. Tan G, Liu S, Wang D, Zhang S (2013) In situ observation of wax-in-oil flow in rough soft contact. Tribol Lett 52(1):93–103
83. Tirella A, Vozzi F, Maria CD, Vozzi G, Sandri T, Sassano D, Cognolato L, Ahluwalia A (2011) Substrate stiffness influences high resolution printing of living cells with an ink-jet system. J Biosci Bioeng 112(1):79–85
84. Tripathi D, Pandey S, Das S (2010) Peristaltic flow of viscoelastic fluid with fractional maxwell model through a channel. Appl Math Comput 215(10):3645–3654
85. Unger MA, Chou HP, Thorsen T, Scherer A, Quake SR (2000) Monolithic microfabricated valves and pumps by multilayer soft lithography. Science 288(5463):113–116
86. Urzay J (2010) Asymptotic theory of the elastohydrodynamic adhesion and gliding motion of a solid particle over soft and sticky substrates at low reynolds numbers. J Fluid Mech 653:391–429
87. Urzay J, Smith SGL, Glover BJ (2007) The elastohydrodynamic force on a sphere near a soft wall. Phys Fluids 19(10):103106
88. Vajravelu K, Sreenadh S, Devaki P, Prasad K (2015) Peristaltic transport of a herschelGbulkley fluid in an elastic tube. Heat TransferGAsian Res 44(7):585–598
89. de Vicente J, Stokes J, Spikes H (2005) The frictional properties of newtonian fluids in rolling-sliding soft-ehl contact. Tribol Lett 20(3):273–286
90. Villey R, Martinot E, Cottin-Bizonne C, Phaner-Goutorbe M, Leger L, Restagno F, Charlaix E (2013) Effect of surface elasticity on the rheology of nanometric liquids. Phys Rev Lett 111:215701
91. Wang X, Bai S, Huang P (2006) Theoretical analysis and experimental study on the influence of electric double layer on thin film lubrication. Front Mech Eng China 1(3):370–373
92. Wang Y, Dhong C, Frechette J (2015) Out-of-contact elastohydrodynamic deformation due to lubrication forces. Phys Rev Lett 115:248302
93. Weaver JA, Melin J, Stark D, Quake SR, Horowitz MA (2010) Static control logic for microfluidic devices using pressure-gain valves. Nat Phys 6:218–223
94. Weekley SJ, Waters SL, Jensen OE (2006) Transient elastohydrodynamic drag on a particle moving near a deformable wall. Quart J Mech Appl Math 59(2):277–300
95. Wexler JS, Trinh PH, Berthet H, Quennouz N, du Roure O, Huppert HE, Lindner A, Stone HA (2013) Bending of elastic fibres in viscous flows: the influence of confinement. J Fluid Mech 720:517–544
96. Wong P, Huang P, Meng Y (2003) The effect of the electric double layer on a very thin water lubricating film. Tribol Lett 14(3):197–203
97. Yin X, Kumar S (2005) Lubrication flow between a cavity and a flexible wall. Phys Fluids 17(6):063101
98. Young A, Bloomstein T, Palmacci S (1999) Contoured elastic-membrane microvalves for microfluidic network integration. J Biomech Eng 121(1):2–6
99. Zhang B, Umehara N (1998) Hydrodynamic lubrication theory considering electric double layer for very thin water film lubrication of ceramics. JSME Int J Ser C 41(2):285–290
100. Zheng Z, Griffiths IM, Stone HA (2015) Propagation of a viscous thin film over an elastic membrane. J Fluid Mech 784:443–G464

Pratyaksh Karan is a Ph.D. student in the Department of Mechanical Engineering at the Indian Institute of Technology (IIT) Kharagpur. He graduated with a dual degree (integrated B.Tech and M.Tech) in mechanical engineering from IIT Kharagpur in 2015. Subsequently, he worked at Flipkart Internet Pvt. Ltd. for a year in the logistics department. His joined the Indian Institute of Technology Kharagpur as a Ph.D. student in January 2017. His area of work includes microfluidics on soft substrate and electrokinetic interactions in microfluidic setups. His research interests include microfluidics, fluids–structure interactions, hydrophobicity, and thermodynamic power cycles.

Jeevanjyoti Chakraborty is an Assistant Professor in the Department of Mechanical Engineering at the Indian Institute of Technology (IIT) Kharagpur. He graduated with a dual degree (integrated B.Tech and M.Tech) in mechanical engineering from IIT Kharagpur in 2009. Subsequently, he completely his Ph.D. in 2013 at IIT Kharagpur itself in the broad area of microfluidics and nanofluidics with focus on electrokinetic flows through narrow confinements. He next worked as a postdoctoral researcher at the Mathematical Institute in the University of Oxford on the mathematical modelling of lithium-ion batteries and then at the School of Mathematics, University of Birmingham (UK) on the mathematical modelling of plant root cell growth. He joined the Indian Institute of Technology Kharagpur as a faculty in 2016. His research interests include modelling combined chemical and mechanical effects in energy storage devices and small-scale flows through deformable confinements.

Suman Chakraborty is a Professor in the Department of Mechanical Engineering at the Indian Institute of Technology Kharagpur. He is currently holding the position of institute chair professor. He is also the Dean, Sponsored Research and Industrial Consultancy and Head, School of Medical Science and Technology at the same Institute. His research interests include microfluidics and nanofluidics, including their theoretical, computational, and experimental modelling, encompassing the underlying fundamentals as well as biomedical, and energy-related, environmental, and other applications. Substantial proportions of his current research projects pertain to bio-microfluidics with focus on technologies for affordable health care. He has been the recipient of many prestigious awards and fellowships, including the Santi Swarup Bhatnagar Prize, fellowships of all the relevant National Academies of Science and Engineering as well as some leading International bodies such as the American Society of Mechanical Engineering, American Physical Society, and Royal Society of Chemistry (UK).